Rapid prototyping of carbon-based chemiresistive gas sensors on paper

Katherine A. Mirica, Joseph M. Azzarelli, Jonathan G. Weis, Jan M. Schnorr, and Timothy M. Swager[1]

Department of Chemistry, Massachusetts Institute of Technology, Cambridge, MA 02139

Contributed by Timothy M. Swager, July 17, 2013 (sent for review March 17, 2013)

Chemically functionalized carbon nanotubes (CNTs) are promising materials for sensing of gases and volatile organic compounds. However, the poor solubility of carbon nanotubes hinders their chemical functionalization and the subsequent integration of these materials into devices. This manuscript describes a solvent-free procedure for rapid prototyping of selective chemiresistors from CNTs and graphite on the surface of paper. This procedure enables fabrication of functional gas sensors from commercially available starting materials in less than 15 min. The first step of this procedure involves the generation of solid composites of CNTs or graphite with small molecule selectors—designed to interact with specific classes of gaseous analytes—by solvent-free mechanical mixing in a ball mill and subsequent compression. The second step involves deposition of chemiresistive sensors by mechanical abrasion of these solid composites onto the surface of paper. Parallel fabrication of multiple chemiresistors from diverse composites rapidly generates cross-reactive arrays capable of sensing and differentiating gases and volatile organic compounds at part-per-million and part-per-thousand concentrations.

mechanochemistry | gas sensor arrays | pencil | nanocarbon | electronic nose

Development of simple and low-cost technologies for detecting and identifying gases and volatile organic compounds (VOCs) is critically important for improving human health, safety, and quality of life (1–3). Carbon nanotubes (CNTs) are promising materials for sensing gases and VOCs because they can be integrated into portable, sensitive, cost-effective, and low-power devices (4–6). The molecular structure of CNTs renders the electrical conductance of these materials extremely sensitive to changes in their local chemical environment (7), and the compatibility of these materials with covalent (8–11) and noncovalent (11, 12) chemical modification enables fabrication of selective sensors (4).

Multiple research groups have exploited several electronic architectures for CNT-based gas and vapor sensors (e.g., chemiresistors, field-effect transistors) with the goal of optimizing various characteristics, such as sensitivity, selectivity, response time and recovery, reproducibility in performance, power requirements, ease of fabrication, and cost (4, 6, 13–15). As a result, various methods have been developed for integrating CNTs into these electronic architectures [e.g., chemical vapor deposition (7, 16), drop casting (17), spin coating (18, 19), spray coating (20, 21), inkjet printing (22, 23), transfer printing (24, 25), and mechanical abrasion (26)]. These methods provide a number of options for integrating CNTs into devices either as individual CNTs, highly aligned arrays of CNTs, or randomly oriented networks of CNTs (4, 6, 13, 15).

Chemiresistors based on randomly oriented networks of CNTs offer significant advantages over other types of architectures for CNT-based sensors in terms of simplicity of design, ease of fabrication, compatibility with chemical functionalization, and sensor-to-sensor reproducibility (27). We (19, 28–30) and others (31–35) have demonstrated several approaches for selective sensing of various gases and VOCs at part-per-million and part-per-billion concentrations using chemiresistive devices based on randomly oriented networks of CNTs. Most of these approaches involve covalent or noncovalent solution-phase chemical functionalization of CNTs to generate selective-sensing materials. To produce devices, the constituent materials are dispersed in a liquid, typically via ultrasonication, and deposited onto electrodes by spin coating, spray coating, or drop casting. The poor solubility of carbon nanotubes in most solvents and the metastability of CNT-based liquid dispersions, however, severely limit the utility and efficiency of these approaches. An enabling addition to the development, prototyping, and fabrication of selective CNT-based sensors and arrays would be a rapid, simple, inexpensive, and solid-state (solvent free) process for chemical functionalization and integration of CNTs into devices.

Here, we describe an entirely solvent-free process for the rapid prototyping of selective CNT- and graphite-based chemiresistive gas and vapor sensors by mechanical abrasion of solid sensing materials on the surface of paper (Fig. 1). This process makes it possible to fabricate functional chemiresistors from commercially available starting materials in less than 15 min. The first step in this process involves the fabrication of a unique class of chemiresistive sensing materials we call "PENCILs" (process-enhanced nanocarbon for integrated logic) and takes less than 10 min (Fig. 1). These materials constitute conductive solid composites of nanostructured carbon (nC) with selectors (S)—commercially available small molecules capable of selective chemical interactions with designated classes of analytes (Scheme 1)—generated by solvent-free ball milling and subsequent compression into the shape of a pellet or conventional pencil "lead." To demonstrate the generality of this approach for making selective-sensing materials from nC, we use three different forms of nC: single-walled carbon nanotubes (SWCNTs), multiwalled carbon nanotubes (MWCNTs), and graphite. The second step involves deposition

Significance

This paper describes a rapid, solvent-free, two-step procedure for the fabrication of selective gas and vapor sensors from carbon nanotubes and graphite on the surface of paper that overcomes challenges associated with solvent-assisted chemical functionalization and integration of these materials into devices. The first step generates solid composites from carbon nanotubes (or graphite) and small molecules (chosen to interact with specific types of gases and vapors) by mechanical mixing and subsequent compression into a form similar to a conventional pencil "lead". The second step uses mechanical abrasion ("drawing") of these solid composites on the surface of paper to generate functional devices. The use of diverse composites yields sensing arrays capable of detecting and differentiating gases and vapors and part-per-million concentrations.

Author contributions: K.A.M., J.M.A., J.G.W., J.M.S., and T.M.S. designed research; K.A.M., J.M.A., and J.G.W. performed research; K.A.M., J.M.A., J.G.W., J.M.S., and T.M.S. analyzed data; and K.A.M., J.M.A., J.G.W., J.M.S., and T.M.S. wrote the paper.

The authors declare no conflict of interest.

[1]To whom correspondence should be addressed. E-mail: tswager@mit.edu.

This article contains supporting information online at www.pnas.org/lookup/suppl/doi:10.1073/pnas.1307251110/-/DCSupplemental.

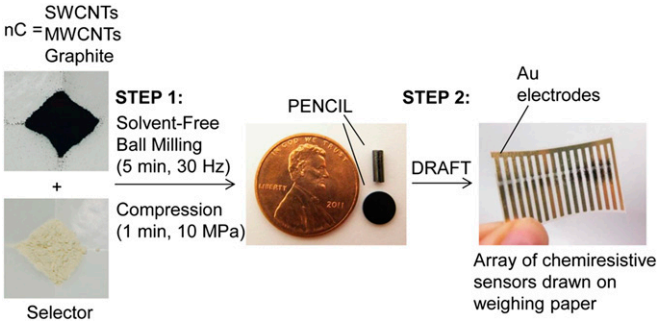

Fig. 1. Schematic outline of the process for rapid prototyping of selective carbon-based chemiresistors on the surface of paper. The process involves two steps. The first step generates PENCILs by mechanical ball milling and subsequent compression of nC with small molecule selectors specifically chosen to interact with target analytes. The second step uses DRAFT to produce an array of chemiresistors on the surface of weighing paper.

of sensing materials on the surface of paper using a method we call "DRAFT" (deposition of resistors with abrasion fabrication technique), and takes less than 5 min. This method is analogous to drawing with pencil on paper, and has been recently reported by our group as a convenient, reliable, and solvent-free method for fabricating ammonia sensors from pristine SWCNTs (26). We now demonstrate the utility and generality of DRAFT by producing arrays of selective chemiresistors by abrasion of PENCILs on the surface of paper.

Design of Devices

The sensors in this study consist of conductive networks of carbon-based sensing materials deposited on the surface of paper-based chips equipped with gold electrodes. We chose to configure our sensors as chemiresistors (i.e., variable resistors that change their resistivity in the presence of chemical analytes) because this type of architecture is the simplest configuration of an electronic sensor. By virtue of their simplicity, chemiresistors have minimal power requirements, and can be readily incorporated into miniaturized multiplexed arrays. We chose cellulose-based paper as the substrate for the fabrication of chemiresistive sensors because it is a ubiquitous and inexpensive material that can be easily integrated into electronic devices (36). The compatibility of paper with several well-established surface-processing technologies [e.g., drawing (26), printing (22, 23), metal evaporation (37), and chemical vapor deposition (38)] facilitates rapid and straightforward introduction of diverse electronic features onto the surface of paper, and integration into chemiresistive sensing devices. Previously, we demonstrated that weighing paper (i.e., highly compressed cellulose) was superior to other types of cellulose-based paper for making ammonia sensors from pristine SWCNTs by DRAFT (26); this demonstration further refined our choice of paper for this study. Although the sensing material itself can also serve as the electrodes in a chemiresistive sensor, it can be beneficial to use metal electrodes for several reasons, such as (*i*) the minimization of the amount of sensing material required to produce a functional chemiresistor; (*ii*) straightforward and rapid integration of devices into arrays; and (*iii*) low contact resistance at electrical connections. We chose gold as the material for the fabrication of electrodes on the surface of paper because it is chemically inert, has low contact resistance, and is easily deposited on the surface of paper by thermal evaporation. To create devices, we first fabricate paper-based chips by depositing electrodes (with thickness of 120 nm, and a gap of 1 mm between electrodes) via thermal evaporation of gold through a shadow mask. We then incorporate chemiresistors onto the surface of the paper-based chip by DRAFT between the gold electrodes. The specific layout of the gold electrodes on paper (Fig. 1) was chosen to facilitate parallel integration of multiple chemiresistors onto a single chip. All sensors in this study have similar resistance (typically ~10–50 kΩ, as measured by a multimeter across the gold electrodes). This feature allows for a chip

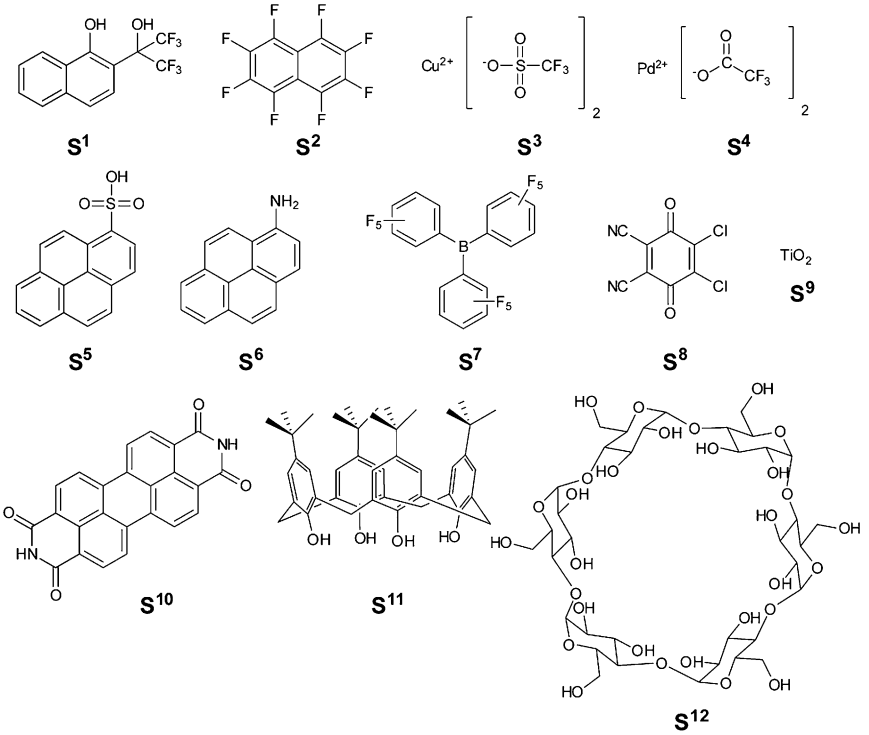

Scheme 1. Structures of selectors [S[1]–S (12)] used in this study.

design with one common counter/reference electrode for all devices. When connected to a portable potentiostat equipped with a multiplexer, this layout permits evaluation of sensing performance of multiple chemiresistors simultaneously (using the same range of output current), and, thus, streamlines the characterization of device-to-device reproducibility and of the cumulative response from cross-reactive arrays. Because different PENCILs display a wide range of conductivities (*SI Appendix*, Table S3), different film thicknesses may be required to obtain devices within the same resistance range.

Fabrication and Characterization of PENCILs

To define optimal characteristics of PENCILs for targeting specific analytes, we began by examining how the type of nC (e.g., graphite, SWCNTs, and MWCNTs) and the concentration of S (i.e., nC:S ratio) affects the materials properties and sensing response of the resulting composites. We focused this study on nC/S composites generated by ball milling selector **1** [S^1] with graphite, SWCNTs, and MWCNTs at four different mass ratios (1:0, 1:1, 1:2, and 1:5) for 5 min at 30 Hz. [Using higher ratios of nC/S (e.g., 1:10) produced composites that were insufficiently conductive for generating functional chemiresistive devices using standardized architectures of devices employed in this study (i.e., bridging a 1-mm gap between gold electrodes to generate devices with R = 10–50 kΩ).] We chose S^1 for this study based on previous demonstrations that covalent and noncovalent incorporation of a hexafluoroisopropyl moiety onto the surface of carbon nanotubes enhances the response of these materials toward O-containing H-bond acceptors, such as dimethyl methylphosphonate (DMMP), tetrahydrofuran, and ketones (19, 29). We hypothesized that the naphthyl moiety within S^1 would enable favorable dispersive interactions with the conjugated sp^2 framework of nC, and the hexafluoroisopropyl moiety would facilitate favorable H-bonding interactions with target analytes (e.g., acetone, THF, and DMMP).

We generated PENCILs from nC/S blends by compression into the shape of a pellet within a stainless steel die for 1 min at 10 MPa (see *SI Appendix* for details). Although fabrication of PENCILs in the shape of a conventional cylindrical pencil lead compatible with commercial mechanical pencil holders is also possible (Fig. 1), molding composites into the shape of a pellet yields a flat surface amenable to various methods of characterization. We characterized the materials properties of the resulting PENCILs using Raman spectroscopy, energy-dispersive X-ray (EDX) spectroscopy, scanning electron microscopy, conductivity measurements, and mechanical analysis.

Raman spectroscopy of PENCILs based on S^1 (*SI Appendix*, Fig. S1) using an excitation wavelength of 633 nm confirmed the presence of graphite, SWCNTs, and MWCNTs within the respective composites with no evidence of significant covalent functionalization of nC with selectors, and no indication of significant exfoliation of graphite into graphene (39). Furthermore, examination of SWCNT/S^1 composites at three different excitation wavelengths (532, 633, and 784 nm) revealed no significant systematic changes in the ratio of intensities of D to G bands (I_D:I_G) with incorporation of S^1 that would be expected in the case of covalent modification of SWCNTs (*SI Appendix*, Fig. S2) (40). In the case of graphite, increasing the concentration of S^1, [S^1], produced a small systematic increase in I_D/I_G. This increase in I_D/I_G may indicate increased disorder of the sp^2 lattice and potential reduction in size of graphite crystallites with increased [S^1] (39). No systematic increase in I_D/I_G was observed for composites of S^1 with MWCNTs (*SI Appendix*, Fig. S1). Raman spectra of composites of S^1 with SWCNTs and graphite also showed a small downshift (1–2 cm^{-1}) in the positions of D and G bands of these nCs with increasing [S^1] within the blend. These downshifts may result from dispersive and doping interactions between S^1 and nC (39, 41). Further analysis of PENCILs with EDX (*SI Appendix*, Figs. S3–S6) revealed uniform dispersion of S^1 and nC within the composite on microscale. To obtain information about the nanoscale structure of the composites, we examined the samples with SEM. Fig. 2 shows high-resolution SEM images of composites of S^1 with graphite, SWCNTs, and MWCNTs at four different mass ratios [nC/S^1 = 1:0, 1:1, 1:2, and 1:5]. The presence of S^1 alters the nanoscopic structure of composites for all forms of nC by coating the surface of SWCNTs, MWCNTs, and graphite crystallites.

The PENCILs were also characterized by conductivity measurements with a four-point probe and mechanical analysis by nanoindentation (see *SI Appendix* for details). PENCILs exhibited a systematic decrease in bulk conductivity with increasing [S^1] [e.g., 256 S/cm for 1:0 SWCNT/S^1, 56 S/cm for 1:1 SWCNT/S^1, 25 S/cm for 1:2 SWCNT/S^1, and 2 S/cm for 1:5 SWCNT/S^1; see *SI Appendix*, Table S1 for details]. This systematic decrease in conductivity (i.e., increase in resistivity) is consistent with the hypothesis that S^1 coats the surface of nC and thus increases the barrier for the transfer of electrons between nC–nC junctions. Mechanical analysis by nanoindentation revealed that the PENCILs based on SWCNT/S^1 and graphite/S^1 composites have a similar range of hardness (~10–500 MPa; see *SI Appendix*, Table S2 for details) to those of conventional commercial graphite-based pencil leads (e.g., 100 MPa for a standard HB pencil) (42). Blending S^1 with nC reduces the hardness of the resulting composite [e.g., from 118 MPa for 1:0 SWCNT/S^1 to 7 MPa for 1:5 SWCNT/S^1].

Sensing Performance of Chemiresistors

After analyzing the materials properties of nC/S^1 composites, we evaluated the performance of these materials as chemiresistive vapor sensors. DRAFT of these composites between gold

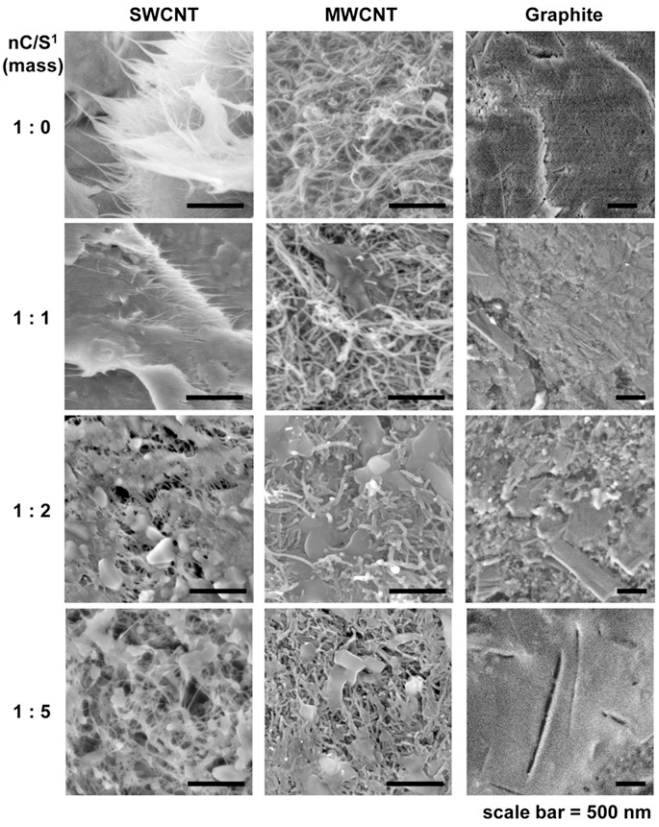

Fig. 2. Characterization of PENCILs based on S^1 blended with SWCNTs, MWCNTs, and graphite using SEM.

electrodes on the surface of weighing paper produced functional devices (typical range of resistance between 10 and 50 kΩ). We evaluated the sensing performance of the devices by applying a constant voltage (0.1 V) across the gold electrodes and monitoring the change in current upon exposure to the target analytes using a potentiostat. The sensing response $-\Delta G/G_0$ (%) was calculated by observing the normalized difference in current before (I_0) and after (I) the exposure to the analyte: $-\Delta G/G_0$ (%) = $[(I_0 - I)/I_0] \times 100$. All sensors (each type in triplicate) were exposed to the analytes for 30 s followed by 170 s recovery under a constant flow of nitrogen (see *SI Appendix* for details). The concentrations of analytes for this experiment were chosen to be sufficiently high (~1% of equilibrium vapor pressure at 25 °C) to obtain a measureable response from the pristine forms of nC. Comparing response of pristine nC to nC/S^1 blends yielded quantitative information about signal enhancement in the presence of S^1 (Fig. 3).

Fig. 3 illustrates that blending S^1 with nC enhances response toward target analytes by up to 1–2 orders of magnitude compared with various forms of pristine nC. For instance, when 1:5 composites (by mass) of MWCNT/S^1, SWCNTs/S^1, and graphite/S^1 are exposed to THF vapor (Fig. 3*B*), we observe 164-fold, 8-fold, and 14-fold enhancement in sensing response, respectively, compared with the corresponding forms of nC in the absence of S^1. We attribute this enhancement in the sensing response to the favorable adsorption of the analytes onto the S^1–coated surface of the nC, and the ability of these nC/S^1 composites to transduce this molecular interaction as a change in electrical properties. The magnitude and reversibility of the sensing response of nC/S^1 composites toward specific analytes is a complex function of three experimental parameters: (*i*) the type of analyte; (*ii*) the type of nC; and (*iii*) nC/S^1 ratio (Fig. 3). Due to their differences in chemical structure, each of the analytes in this study has a unique set of kinetic and thermodynamic constants that drive its molecular association and dissociation with the S^1–coated surface of nC. In addition, differences between the ability of the different analytes to partition and diffuse into the solid composite may also contribute to the differences in analyte-specific sensing responses. Comparing Fig. 3, *Left, Center*, and *Right* reveals how the type of analyte (acetone vs. THF vs. DMMP) influences the sensing response of devices. The sensors exhibit a reversible response toward acetone and THF (Fig. 3 *A* and *B*), and only a partially reversible response toward DMMP on the time scale of the experiment (Fig. 3*C*). We attribute these differences in reversibility to the differences in the kinetic and thermodynamic parameters that characterize the interaction of the analytes with the S^1–coated surface of each nC.

Fig. 3 also yields information about how the type of nC (graphite vs. SWCNTs vs. MWCNTs) and the nC/S^1 ratio influences the sensing response of devices. In general, systematically increasing [S^1] within the composites increases the sensing response of the corresponding devices toward acetone and THF (Fig. 3 *A*, *B*, *D*, and *E*). In contrast, the enhancement in sensing response of the devices toward DMMP has a less systematic dependence on [S^1] within the blend (Fig. 3*F*). It is interesting to note that the magnitude of the sensing response of graphite/S^1 composites toward DMMP is comparable to those based on much more expensive forms of carbon, such as SWCNT/S^1 and MWCNT/S^1 (Fig. 3*F*). The dependence of sensing response on the type of nC can be attributed to the differences in: (*i*) the surface-to-volume ratio of individual particles of nC, (*ii*) the length and the number of available conduction pathways within the composite, and (*iii*) the efficiency of mixing between S^1 and nC within the composite. Although further experiments would be needed to enable rational selection of the optimal type of nC for targeting specific analytes, it is clear that nC/S ratio within the composite [at least 1:2 or 1:5 by mass in the case nC/S^1] is a crucial parameter for maximizing the response of the sensors toward target analytes.

Rapid Prototyping of Selective Sensors within Cross-Reactive Arrays

To demonstrate the generality of the process for fabricating selective gas and vapor sensors from PENCILs by DRAFT, we constructed an array of cross-reactive sensors (see *SI Appendix*, Fig. S7 for a photograph of selected sensors within the array). This arrayed format is modular, straightforward to implement, and facilitates evaluation of sensing performance of multiple devices simultaneously. Each sensor within the array comprises a solid composite of SWCNTs with a specific S (1:4 by mass) deposited on the surface of weighing paper by DRAFT; an additional sensor based on pristine ball-milled SWCNTs serves as a control for evaluating enhancements in sensitivity and selectivity of the SWCNT/S composites toward specific analytes. We chose SWCNT-based composites for this study because their chemical structure containing exclusively surface atoms makes them particularly attractive for sensing applications.

Fig. 4 summarizes the magnitude of the sensing response of five chemically distinct sensors toward 10 different analytes. Each sensing response represents the average change in conductance $-\Delta G/G_0$ (%) from three devices fabricated using the

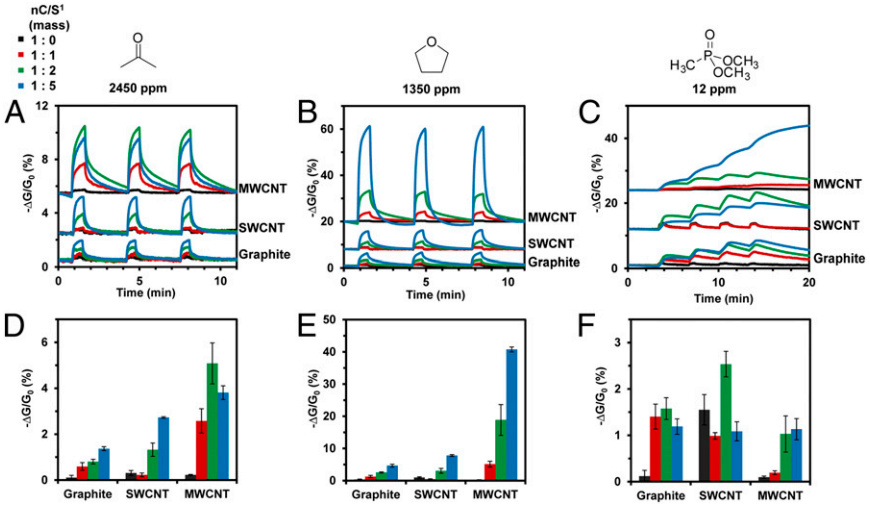

Fig. 3. Response toward acetone, THF, and DMMP of sensors fabricated on the surface of weighing paper by mechanical abrasion of PENCILs comprising compressed blends of nC (graphite, SWCNTs, and MWCNTs) and S^1 at different mass ratios (1:0, 1:1, 1:2, and 1:5). Change in conductance (represented as $-\Delta G/G_0$, %) with time of devices exposed to acetone (*A*), THF (*B*), and DMMP (*C*) for 30 s. Quantitative comparison of sensing response ($-\Delta G/G_0$, %) toward acetone (*D*), THF (*E*), and DMMP (*F*) for three different forms of nC (graphite, SWCNT, and MWCNT) blended with S^1 at four different mass ratios (1:0, 1:1, 1:2, and 1:5). Vertical error bars represent SD from the mean based on three exposures of three sensors to each of the analytes.

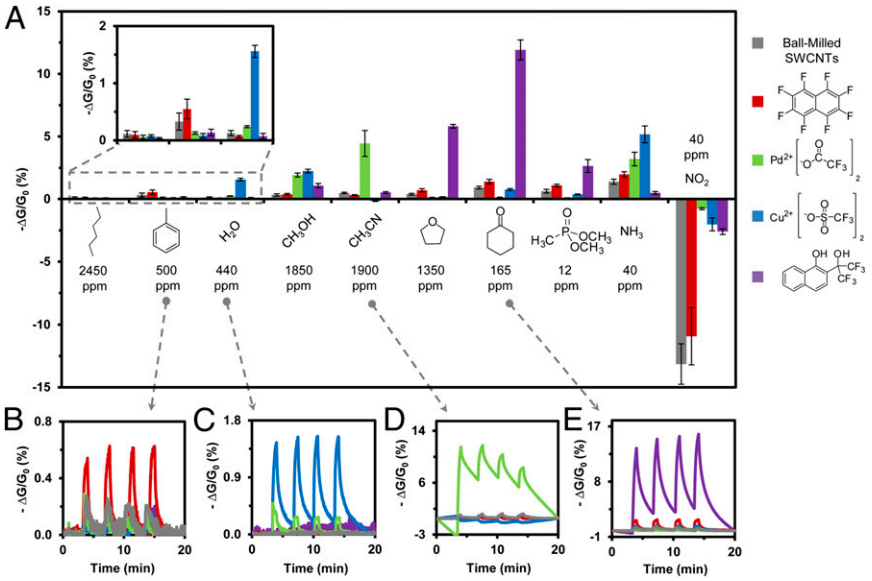

Fig. 4. Sensing response of a cross-reactive array fabricated by mechanical abrasion of ball milled and compressed SWCNTs and composites of SWCNTs with selectors S^1–S (4) with (1:4 nC/S by mass) on the surface of weighing paper. (*A*) Change in conductance (represented as $-\Delta G/G_0$, %) resulting from exposure of the array to eight vapors (at ~1% equilibrium vapor pressure, specific concentrations as shown) and two gases (40 ppm each). Each bar represents the average response of three sensors exposed to each analyte in triplicate. Vertical error bars show SD from the mean based on three exposures of three sensors to each of the analytes. (*B*) S (2) exhibits enhanced signal toward toluene. (*C*) S (3) shows enhanced signal toward water vapor. (*D*) S (4) enhances signal toward acetonitrile. (*E*) S^1 enhances signal toward cyclohexanone.

same PENCIL and simultaneously exposed to each analyte at least three times (nine total measurements). Compared with SWCNT control, incorporation of selectors S^1–S (4) into SWCNT composites produced devices with enhanced selectivity and sensitivity toward selected analytes. For instance, incorporation of S^1 (an H-bond donor) enhanced sensitivity toward H-bond acceptors (e.g., 15× for THF, 13× for cyclohexanone, and 4× for DMMP), S (2) enhanced sensitivity toward electron-rich aromatics (e.g., 2× for toluene), S (3) (a Lewis acid) enhanced sensitivity toward Lewis bases (e.g., 12× for H_2O, 7× for CH_3OH, and 4× for NH_3,), while S (4) enhanced sensitivity toward CH_3OH (6×) and CH_3CN (9×) with respect to the SWCNT control. *SI Appendix*, Figs. S8 and S9 show the sensing response of additional selectors [S (5)–S (12)] examined in this study. Compared with pristine SWCNTs, composites of these selectors with SWCNTs showed increased selectivity, but no large enhancements in sensitivity compared with unmodified SWCNTs toward target analytes.

To probe the generality of this method for various forms of nC, we also constructed an array of cross-reactive sensors from graphite-based composites with S^1 – S (12) (1:4 graphite/S by mass). *SI Appendix*, Figs. S10 and S11 show the sensing response of the devices based on these composites toward various analytes. *SI Appendix*, Fig. S12 summarizes the quantitative sensing response for selected devices and analytes. Analogous to the SWCNT-based array, blending of selectors S^1, S (3), and S (4) with graphite produced sensing materials and devices with enhanced selectivity and sensitivity toward selected analytes. It is notable that these graphite-based sensing materials showed enhanced selectivity and sensitivity toward target analytes in comparison with both graphite and SWCNT controls (*SI Appendix*, Fig. S13). Although SWCNT-based composites with selectors S^1–S (4) exhibited higher sensing response toward the target analytes compared with their graphite-based analogs (*SI Appendix*, Fig. S13), the results summarized in *SI Appendix*, Fig. S13 suggest that inexpensive forms of carbon, such as graphite, can be readily used for solvent-free rapid prototyping and identification of selective chemiresistive sensing materials based on binary mixtures of selectors and nC. Once these selective materials have been identified, optimization of the source of nC can yield materials and devices with enhanced chemical properties for specific applications.

Discrimination of Analytes Using Principal Component Analysis

To evaluate the ability of the sensor arrays fabricated on paper from PENCILs by DRAFT to identify and discriminate different gases and VOCs, we examined the sensing results using principal component analysis (PCA) (43). Fig. 5 shows the ability of the five-sensor SWCNT-based array presented in Fig. 4 to resolve 10 chemically diverse analytes using the first three principal components (PCs). *SI Appendix*, Fig. S14 also illustrates this resolution of analytes using 2D projections of PCs. In addition, *SI Appendix*, Fig. S15 shows the analogous capability of the graphite- and SWCNT-based arrays, comprising composites with selectors S^1–S (4) to resolve nine different analytes using the first three PCs of each array.

Conclusion

We developed a simple and versatile method for fabricating selective chemiresistive sensors from graphitic materials on the surface of paper. As part of this approach, we made and characterized a class of sensing materials that comprise solid composites of small molecule selectors with nanostructured carbon (i.e., graphite, SWCNTs, and MWCNTs) generated by mechanical mixing and subsequent compression. We demonstrated that these sensing materials can be designed and produced from at

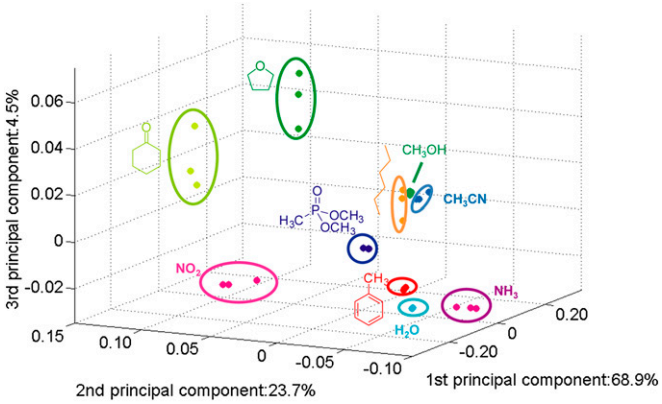

Fig. 5. PCA of a cross-reactive array shown in Fig. 4.

least three different forms of nC, and can be easily integrated into functional chemiresitive gas sensors and cross-reactive arrays by mechanical abrasion on the surface of paper. This approach has at least three advantages over standard technologies based on solution-phase processing of graphitic materials into functional and selective sensing devices: (*i*) It is entirely solvent-free. It does not require the use of toxic solvents, surfactants, or prolonged sonication for dispersing materials in solution, and integration into devices. (*ii*) It is rapid. The entire process of fabricating a functional selective chemiresistors from commercially available starting materials takes less than 15 min (the fabrication of PENCILs takes less than 10 min, and DRAFT takes less than 5 min). In contrast, covalent and noncovalent functionalization of CNTs to generate selective sensing materials in solution takes hours (and sometimes days), and integration of these materials into devices by drop casting, spin coating, and inkjet printing requires prolonged drying times to remove solvent, and often involves several repeated processing cycles to obtain devices with desired electrical properties. (*iii*) It uses solid composite-sensing materials that have the potential to be more stable than most liquid dispersions of CNTs. One current disadvantage of this method over liquid-based methods is that it requires at least ∼30 mg of material for the fabrication of a single PENCIL. This amount of material is necessary to facilitate straightforward fabrication and abrasion of PENCIL on the surface of paper. This PENCIL, however, can be used repeatedly for the fabrication of multiple sensors by DRAFT (each functional sensor comprises < 5 μg of chemiresistive sensing material). Furthermore, the ability to use graphite as an effective source of carbon for rapid identification of selective solid composites for detecting target analytes may help to circumvent the need for using expensive sources of carbon (i.e., SWCNTs) during preliminary prototyping. We believe that this method will be readily adaptable for the fabrication of selective and sensitive carbon-based sensors and arrays for detecting a wide variety of analytes.

ACKNOWLEDGMENTS. K.A.M. thanks Dr. Birgit Esser for helpful discussions, Dr. Joseph J. Walish for the fabrication of stainless steel mold for compressing materials into the shape of a pencil lead compatible with standard mechanical pencil holders, and Dr. Alan Schwartzman for the assistance with hardness measurements by nanoindentation. The authors thank Nano-C for kindly providing SWCNTs for this project. This research was supported by the Army Research Office through the Institute for Soldier Nanotechnologies, and the National Institutes of Health under Ruth L. Kirschstein National Research Service Award F32CA157197 from the National Cancer Institute (to K.A.M.).

1. Potyrailo RA, Surman C, Nagraj N, Burns A (2011) Materials and transducers toward selective wireless gas sensing. *Chem Rev* 111(11):7315–7354.
2. Stitzel SE, Aernecke MJ, Walt DR (2011) Artificial noses. *Annu Rev Biomed Eng* 13: 1–25.
3. Wilson AD, Baietto M (2009) Applications and advances in electronic-nose technologies. *Sensors* 9(7):5099–5148.
4. Kauffman DR, Star A (2008) Carbon nanotube gas and vapor sensors. *Angew Chem Int Ed Engl* 47(35):6550–6570.
5. Schnorr JM, Swager TM (2011) Emerging applications of carbon nanotubes. *Chem Mater* 23:646–657.
6. Hu LB, Hecht DS, Grüner G (2010) Carbon nanotube thin films: Fabrication, properties, and applications. *Chem Rev* 110(10):5790–5844.
7. Kong J, et al. (2000) Nanotube molecular wires as chemical sensors. *Science* 287(5453): 622–625.
8. Bahr JL, Tour JM (2002) Covalent chemistry of single-wall carbon nanotubes. *J Mater Chem* 12:1952–1958.
9. Zhang W, et al. (2009) Modular functionalization of carbon nanotubes and fullerenes. *J Am Chem Soc* 131(24):8446–8454.
10. Zhang W, Swager TM (2007) Functionalization of single-walled carbon nanotubes and fullerenes via a dimethyl acetylenedicarboxylate-4-dimethylaminopyridine zwitterion approach. *J Am Chem Soc* 129(25):7714–7715.
11. Karousis N, Tagmatarchis N, Tasis D (2010) Current progress on the chemical modification of carbon nanotubes. *Chem Rev* 110(9):5366–5397.
12. Britz DA, Khlobystov AN (2006) Noncovalent interactions of molecules with single walled carbon nanotubes. *Chem Soc Rev* 35(7):637–659.
13. Cao Q, Rogers JA (2009) Ultrathin films of single-walled carbon nanotubes for electronics and sensors: A review of fundamental and applied aspects. *Adv Mater* 21:29–53.
14. Lee BY, et al. (2011) Universal parameters for carbon nanotube network-based sensors: can nanotube sensors be reproducible? *ACS Nano* 5(6):4373–4379.
15. Snow ES, Perkins FK, Robinson JA (2006) Chemical vapor detection using single-walled carbon nanotubes. *Chem Soc Rev* 35(9):790–798.
16. Kang SJ, et al. (2007) High-performance electronics using dense, perfectly aligned arrays of single-walled carbon nanotubes. *Nat Nanotechnol* 2(4):230–236.
17. Li J, et al. (2003) Carbon nanotube sensors for gas and organic vapor detection. *Nano Lett* 3:929–933.
18. Lemieux MC, et al. (2009) Solution assembly of organized carbon nanotube networks for thin-film transistors. *ACS Nano* 3(12):4089–4097.
19. Wang F, Swager TM (2011) Diverse chemiresistors based upon covalently modified multiwalled carbon nanotubes. *J Am Chem Soc* 133(29):11181–11193.
20. Bekyarova E, et al. (2005) Electronic properties of single-walled carbon nanotube networks. *J Am Chem Soc* 127(16):5990–5995.
21. Lipomi DJ, et al. (2011) Skin-like pressure and strain sensors based on transparent elastic films of carbon nanotubes. *Nat Nanotechnol* 6(12):788–792.
22. Ammu S, et al. (2012) Flexible, all-organic chemiresistor for detecting chemically aggressive vapors. *J Am Chem Soc* 134(10):4553–4556.
23. Vyas R, et al. (2011) Inkjet printed, self powered, wireless sensors for environmental, gas, and authentication-based sensing. *IEEE Sens J* 11:3139–3152.
24. Meitl MA, et al. (2004) Solution casting and transfer printing single-walled carbon nanotube films. *Nano Lett* 4:1643–1647.
25. Zhou YX, Hu LB, Gruner G (2006) A method of printing carbon nanotube thin films. *Appl Phys Lett* 88(12):123109.
26. Mirica KA, Weis JG, Schnorr JM, Esser B, Swager TM (2012) Mechanical drawing of gas sensors on paper. *Angew Chem Int Ed Engl* 51(43):10740–10745.
27. Gruner G (2006) Carbon nanotube films for transparent and plastic electronics. *J Mater Chem* 16:3533–3539.
28. Esser B, Schnorr JM, Swager TM (2012) Selective detection of ethylene gas using carbon nanotube-based devices: Utility in determination of fruit ripeness. *Angew Chem Int Ed Engl* 51(23):5752–5756.
29. Wang F, Gu HW, Swager TM (2008) Carbon nanotube/polythiophene chemiresistive sensors for chemical warfare agents. *J Am Chem Soc* 130(16):5392–5393.
30. Wang F, Yang Y, Swager TM (2008) Molecular recognition for high selectivity in carbon nanotube/polythiophene chemiresistors. *Angew Chem Int Ed Engl* 47(44):8394–8396.
31. Bekyarova E, et al. (2004) Chemically functionalized single-walled carbon nanotubes as ammonia sensors. *J Phys Chem B* 108:19717–19720.
32. Ding MN, Sorescu DC, Kotchey GP, Star A (2012) Welding of gold nanoparticles on graphitic templates for chemical sensing. *J Am Chem Soc* 134(7):3472–3479.
33. Peng G, Tisch U, Haick H (2009) Detection of nonpolar molecules by means of carrier scattering in random networks of carbon nanotubes: toward diagnosis of diseases via breath samples. *Nano Lett* 9(4):1362–1368.
34. Peng G, Trock E, Haick H (2008) Detecting simulated patterns of lung cancer biomarkers by random network of single-walled carbon nanotubes coated with nonpolymeric organic materials. *Nano Lett* 8(11):3631–3635.
35. Zilberman Y, Ionescu R, Feng X, Müllen K, Haick H (2011) Nanoarray of polycyclic aromatic hydrocarbons and carbon nanotubes for accurate and predictive detection in real-world environmental humidity. *ACS Nano* 5(8):6743–6753.
36. Tobjörk D, Österbacka R (2011) Paper electronics. *Adv Mater* 23(17):1935–1961.
37. Siegel AC, et al. (2010) Foldable printed circuit boards on paper substrates. *Adv Funct Mater* 20:28–35.
38. Barr MC, et al. (2011) Direct monolithic integration of organic photovoltaic circuits on unmodified paper. *Adv Mater* 23(31):3499–3505.
39. Saito R, Hofmann M, Dresselhaus G, Jorio A, Dresselhaus MS (2011) Raman spectroscopy of graphene and carbon nanotubes. *Adv Phys* 60:413–550.
40. Hof F, Bosch S, Englert JM, Hauke F, Hirsch A (2012) Statistical Raman spectroscopy: A method for the characterization of covalently functionalized single-walled carbon nanotubes. *Angew Chem Int Ed Engl* 51(47):11727–11730.
41. Rao AM, Eklund PC, Bandow S, Thess A, Smalley RE (1997) Evidence for charge transfer in doped carbon nanotube bundles from raman scattering. *Nature* 388: 257–259.
42. Atkins T (2009) *The Science and Engineering of Cutting: The Mechanics and Processes of Separating, Scratching and Puncturing Biomaterials, Metals and Non-Metals* (Elsevier, Oxford, UK).
43. Jolliffe IT (2002) *Principal Component Analysis* (Springer, New York).

SUPPORTING INFORMATION

for

Rapid Prototyping of Carbon-Based Chemiresistive Gas Sensors on Paper

Katherine A. Mirica, Joseph M. Azzarelli, Jonathan G. Weis, Jan M. Schnorr,

and Timothy M. Swager*

Department of Chemistry, Massachusetts Institute of Technology

77 Massachusetts Ave., Cambridge, MA 02139

* Corresponding author: Timothy M. Swager (tswager@mit.edu)

MATERIALS AND METHODS

General Materials and Methods. All chemicals and reagents were purchased from Sigma-Aldrich (Atlanta, GA) and used without further purification, unless noted otherwise. SWCNTs (purified ≥ 95% as SWCNT) were kindly provided by Nano-C, Inc. (Westwood, MA). MWCNTs (> 95 % carbon, outer diameter = 6–9 nm, average length = 5 μm, number of walls = 3–6) were purchased from Sigma-Aldrich (Atlanta, GA). Graphite Powder (natural, microcrystal grade, average particle size of 2-15 microns, 99.9995% [metal basis]) and Octafluoronaphthalene (CAS 313-72-4), 97% were purchased from Alfa Aesar (Ward Hill, MA). 2-(2-Hydroxy-1,1,1,3,3,3-hexafluoropropyl)-1-naphthol (CAS 2092-87-7), 97% was purchased from either SynQuest (Alachua, FL) or Santa Cruz Biotechnology (Santa Cruz, CA). Weighing Paper (Cat. No. 12578-165)—the substrate for the fabrication of sensors by mechanical abrasion— was purchased from VWR International (West Chester, PA). NH_3 (1% in N_2) and NO_2 (1% in air) were custom-ordered from Airgas.

Evaporation of Gold on Paper. Au electrodes (120 nm thickness) were deposited on the surface of paper through a stainless steel shadow mask (purchased from Stencils Unlimited, Lake Oswego, OR, http://www.stencilsunlimited.com/) using Thermal Evaporator (Angstrom Engineering, Kitchener, Ontario, Canada) under pressure of $1–4 \times 10^{-5}$ Torr and a rate of evaporation of 1–2 Å/s.

Ball Milling. Selective sensing materials were generated by solvent-free ball milling of carbon (e.g., SWCNTs) with commercial small molecule "selectors" using an oscillating mixer mill

(MM400, Retsch GmbH, Haan, Germany) within a stainless steel milling vial (5 mL) equipped with a single stainless steel ball (7 mm diameter). Unless otherwise indicated, a typical experiment involved filling the milling vial with carbon powder (e.g., SWCNTs) and selector (total mass of powder = 150 mg) and ball milling the mixture for 5 min at 30 Hz.

Fabrication of PENCILs. PENCILs were fabricated by loading powdered material into a mold, such as a pressing die set with 6-mm internal diameter (Across International, acrossinternational.com, Item # SDS6), or a pressing die set with 13-mm internal diameter (Sigma-Aldrich), or a custom-build die set with 2-mm internal diameter, and compressing the powder by applying a constant pressure of 10 MPa for 1 min using a Hydraulic Press (Carver, Model # 3912 or Across International Item # MP24A).

Fabrication of Sensors by DRAFT. Sensing materials were deposited on the surface of paper between gold electrodes by manual abrasion of the PENCIL. This process involved holding the 13-mm diameter pellet with a double gloved hand between the index finger and the thumb and manually rubbing the pellet on the surface of paper between the gold electrodes at a rate of ~ 10 mm/s with an applied force of ~ 1–5 N (estimated by abrading the pellet on the surface of paper using an analytical balance) several times to obtain the desired resistance of devices (typically ~10–50 kΩ). Precise control over the rate of deposition or the applied force was not necessary; we obtained good reproducibility in sensing response between devices examined in this study. Caution: Dust from carbon nanotubes and selectors may be harmful upon inhalation. To prevent potential inhalation of dust particles generated by the abrasion of PENCIL on paper, fabrication

of devices was carried out in a fume hood or on a benchtop while wearing a respirator face mask and safety glasses.

Sensing Measurements. The array of devices was mounted onto a 25 mm x 75 mm x 1 mm glass slide using a double-sided Scotch tape. The array was then inserted into a 2 x 30 pin edge connector (DigiKey), which made electrical contacts with each of the gold electrodes within the array. The edge connector was then connected to the potentiostat via a breadboard (DigiKey). For sensing measurements, the devices were enclosed within a custom-made gas-tight Teflon chamber containing an inlet and outlet port for gas flow. The inlet port was connected to a gas delivery system, and the outlet port was connected to an exhaust vent. Measurements of conductance were performed under a constant applied voltage of 0.1 V using PalmSense EmStat-MUX equipped with a 16-channel multiplexer (Palm Instruments BV, The Netherlands, http://www.palmsens.com/). Data acquisition was done using PSTrace 2.4 software provided by Palm Instruments. Matlab (R2011a, Mathworks) and Microsoft Excel were used to perform baseline correction, calculate relative sensing responses, and perform principal component analysis. Because some sensors showed partially reversible response toward certain analytes, where the magnitude of the sensing response from the first exposure to the analyte is significantly larger than the response from subsequent exposures, the sensing response of all sensors resulting from the first exposure to all analytes was excluded from calculating the average sensing response and the standard deviation.

Dilution of Gases. Delivery of controlled concentration of gases (NH_3 and NO_2) to devices were performed using Smart-Trak Series 100 (Sierra Instruments, Monterey, CA) gas mixing system at total flow rates of 1 L/min. NH_3 was diluted with N_2, and NO_2 was diluted with air.

Dilution of Vapors. Delivery of controlled concentrations of vapors to devices was carried out using Precision Gas Standards Generator Model 491M-B (Kin-Tek Laboratories, La Marque, TX). All vapors were diluted with N_2 at total flow rates of 0.25–0.50 L/min.

Microscopy. Scanning electron microscopy (SEM) was carried out using a JEOL JSM-6060 or JEOL JSM-6700F field emission SEM (FESEM) with energy-dispersive X-ray spectroscopy (EDX). Typical accelerating voltages were 1.5-5.0 kV.

Raman Spectroscopy. Raman spectra of solid composites of S^1 with various forms of nC were measured on a Horiba LabRAM HR Raman Spectrometer using excitation wavelength of 633 nm. Additional spectra were obtained for SWCNT/S^1 composites using excitation wavelengths of 532 nm and 784 nm. The spectra were collected with the following parameters in place: filter = none; hole = 1000 μm; slit = 100 μm; grating = 600; objective = 10x. In real-time-display mode, the spectral signal at 0 cm^{-1} was zeroed prior to acquisition. The spectrum was collected from 200 cm^{-1} to 3000 cm^{-1} with an integration time of 5 s averaged 100 times.

Measurements of Hardness of PENCILs. Ball-milled blends were compressed into pellets with thickness of ~1 mm using a hydraulic press. Measurements of mechanical hardness were carried out using Hysitron TriboIndenter equipped with a Berkovitch tip using quasi-static

indentation with typical applied loads ranging between 2–10 mN and depth of indentation ranging between 0.5 and 5 μm.

Measurements of Resistivity. Measurements of bulk conductance of compressed blends were carried out using an osmium four-point probe (Signatone, Part number: SP4-50-045-OFS) with a tip radius of 0.127 mm, space between tips of 1.27 mm, and spring pressure of 45 grams. Bulk conductance σ (S/cm) of samples was calculated using Eq. 1. In this equation, V (V) is the voltage, I (A) is the current, w (cm) is the thickness of a circular sample composite, C (unitless) is the geometry correction factor that accounts for a finite diameter of a circular sample composite, and F (unitless) is the thickness correction factor that accounts for a finite thickness of a circular sample composite.[1, 2]

$$\sigma = \mathrm{I}/(V \times w \times C \times \mathrm{F}) \quad (1)$$

Figure S1. Raman Spectroscopy of PENCILs (excitation wavelength = 632.7 nm) based on different mass ratios of S^1 with graphite, SWCNTs, and MWCNTs.

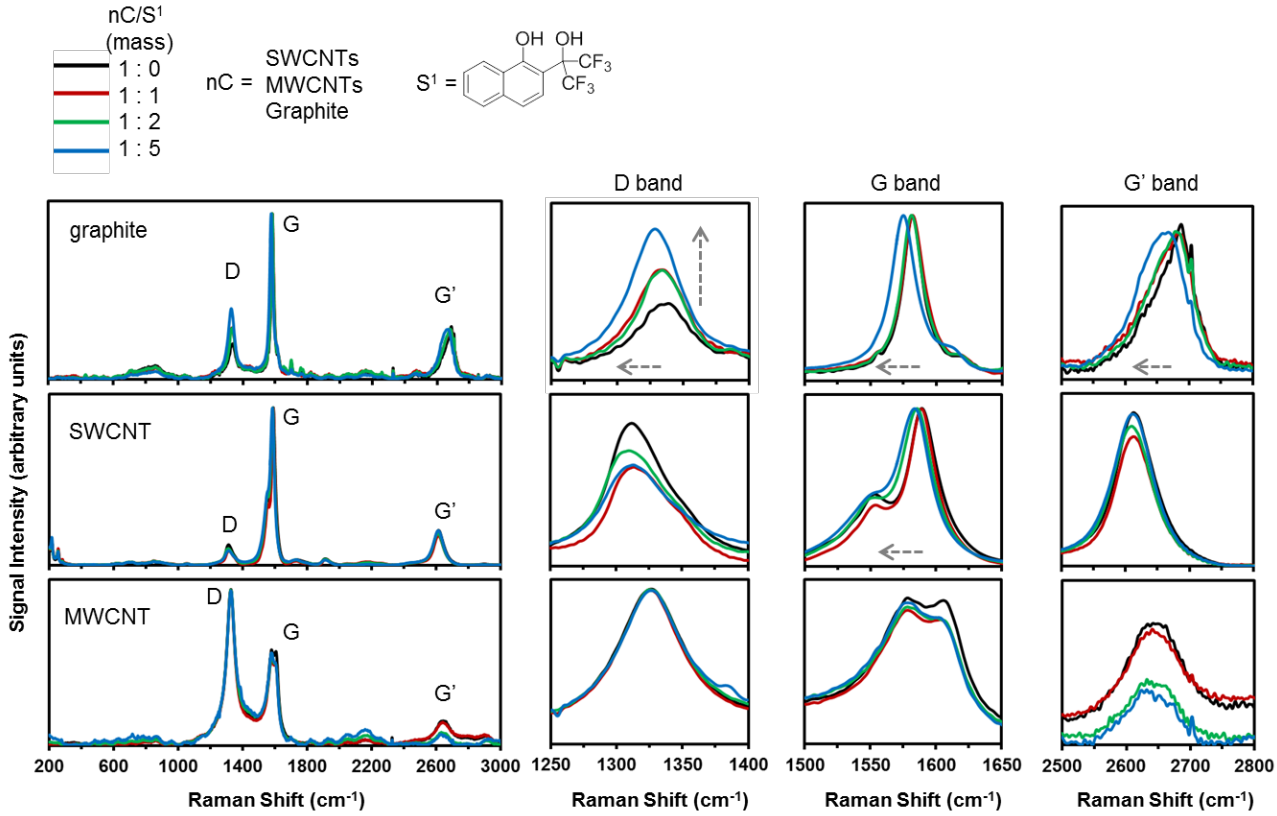

Figure S2. Raman Spectroscopy of SWCNT/S[1] composites at different excitation wavelengths.

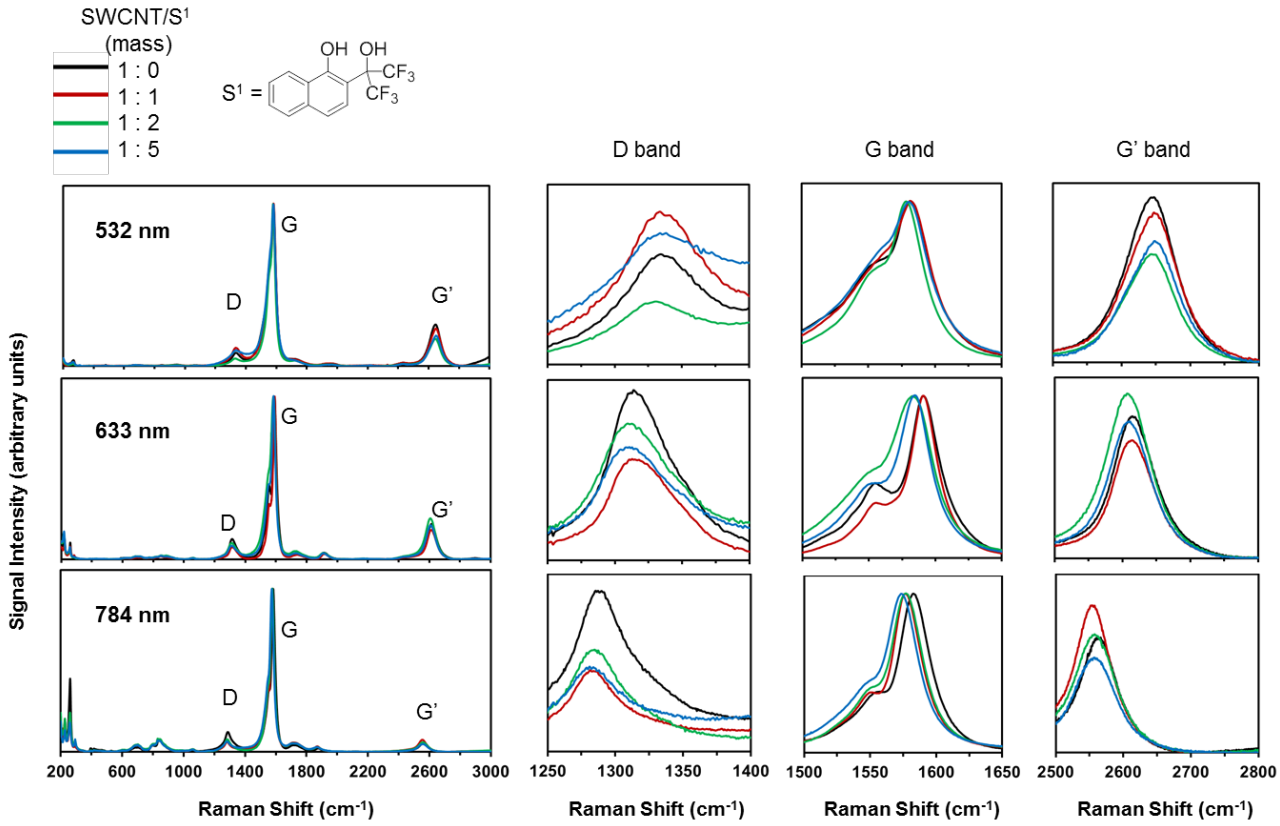

Figure S3. X-Ray survey scans of nC/S[1]composites.

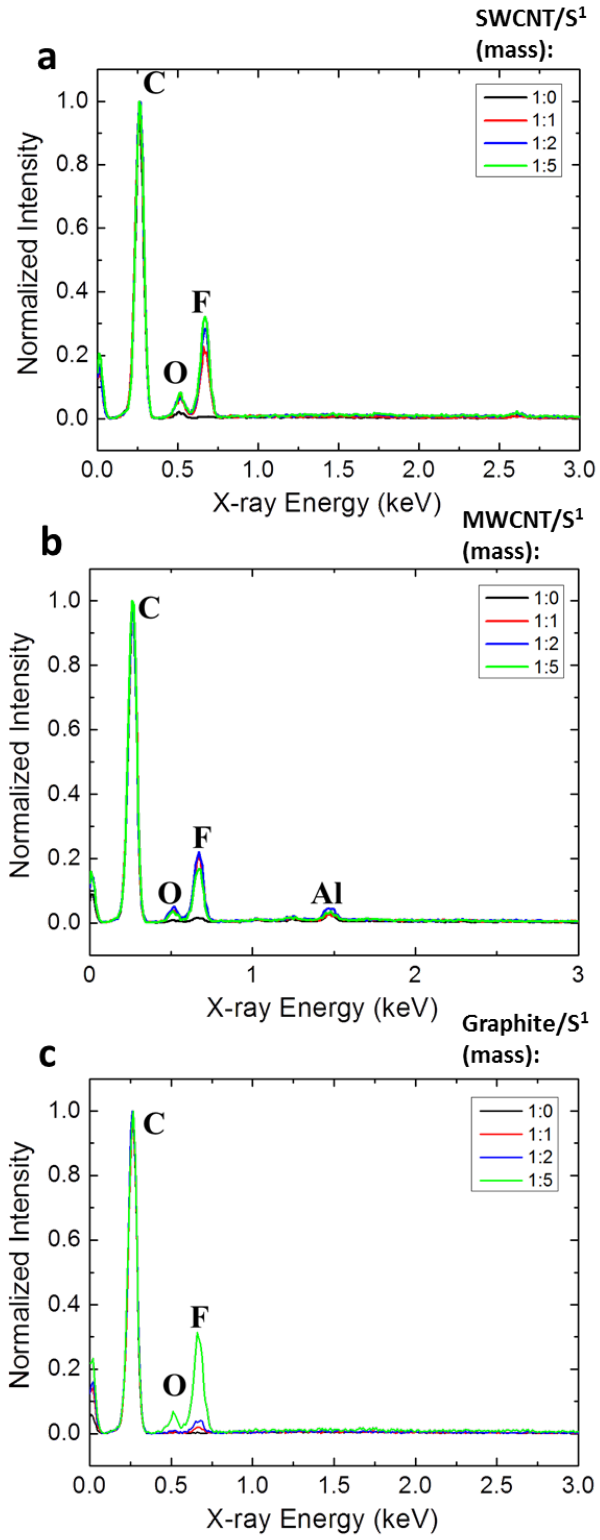

Figure S4. EDX of SWCNT/S[1] composites.

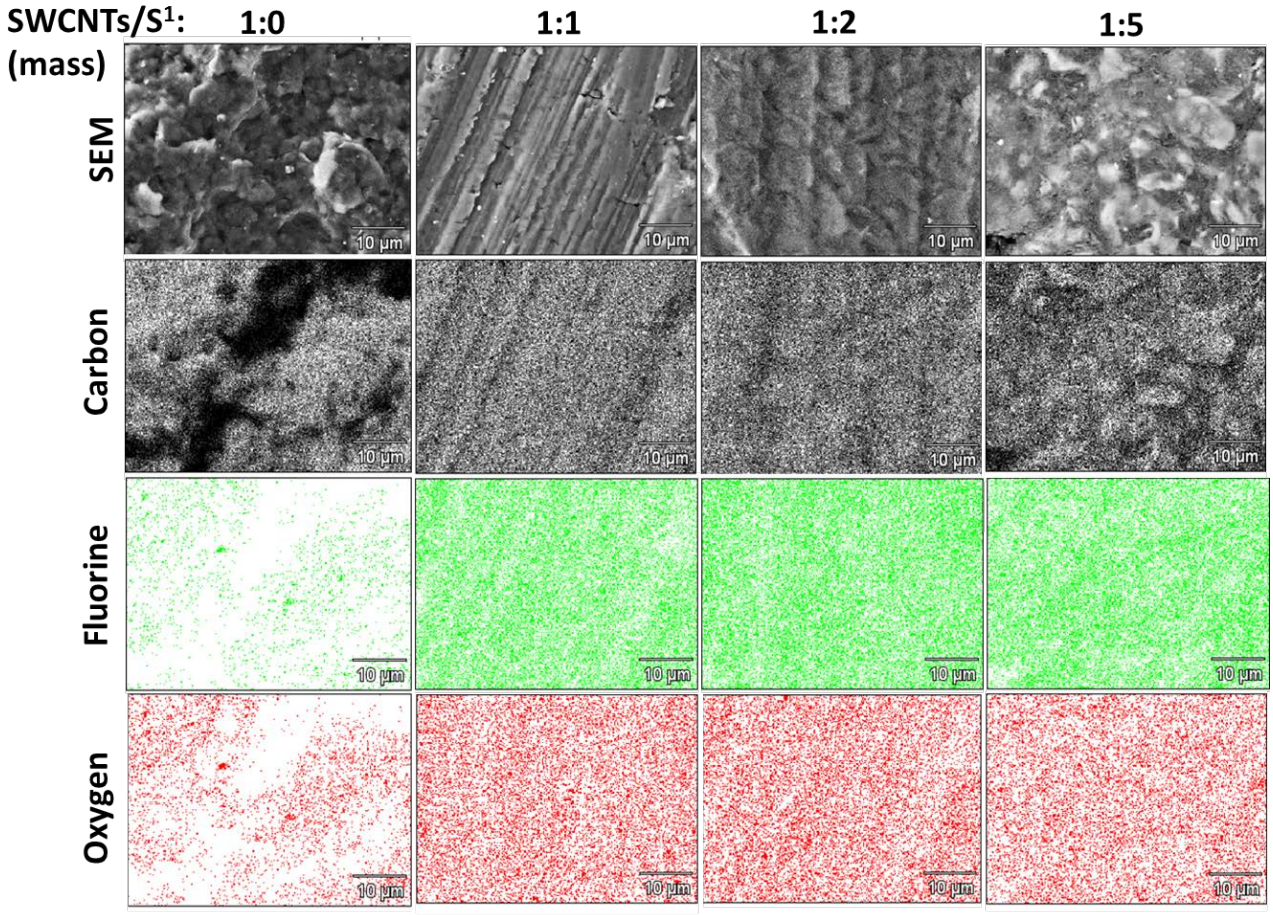

Figure S5. EDX of MWCNT/S[1] composites.

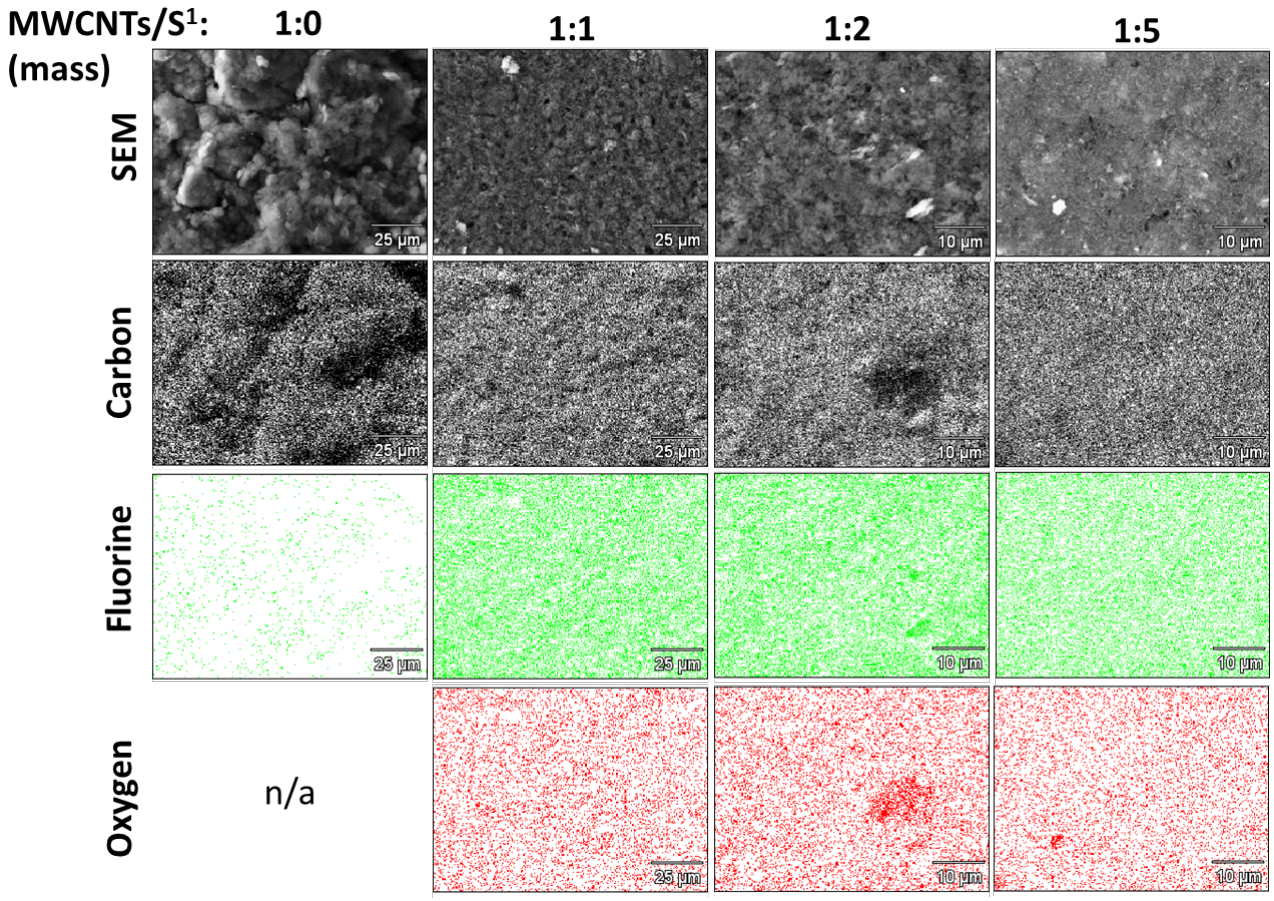

Figure S6. EDX of Graphite/S[1] composites.

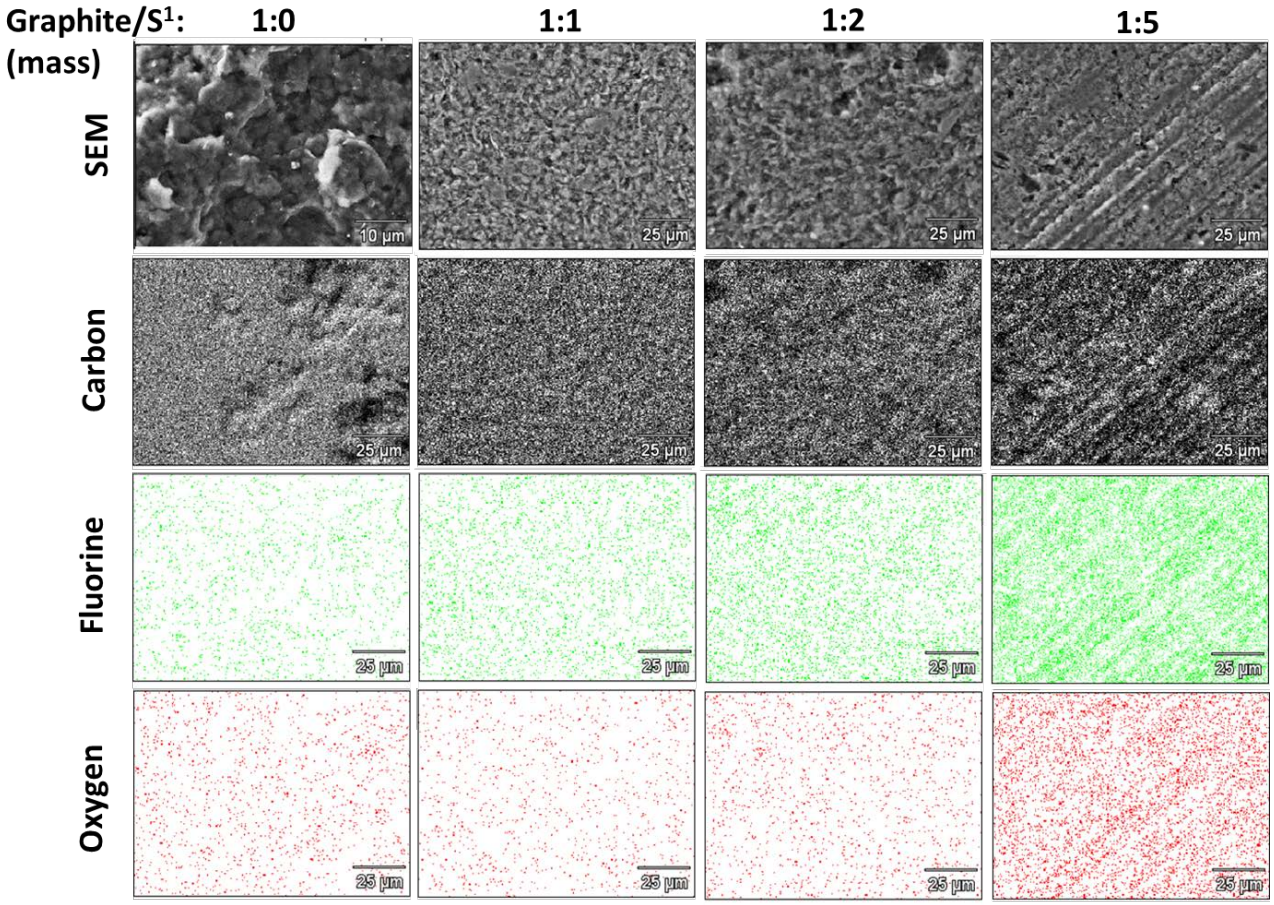

Figure S7. Photograph of selected sensors from the SWCNT-based array. Each sensor is drawn in triplicate on the surface of a paper chip between gold electrodes. Typical resistance range of sensors is 10 – 50 kΩ. The photograph shows two paper chips mounted on the surface of a glass slide using double sided tape.

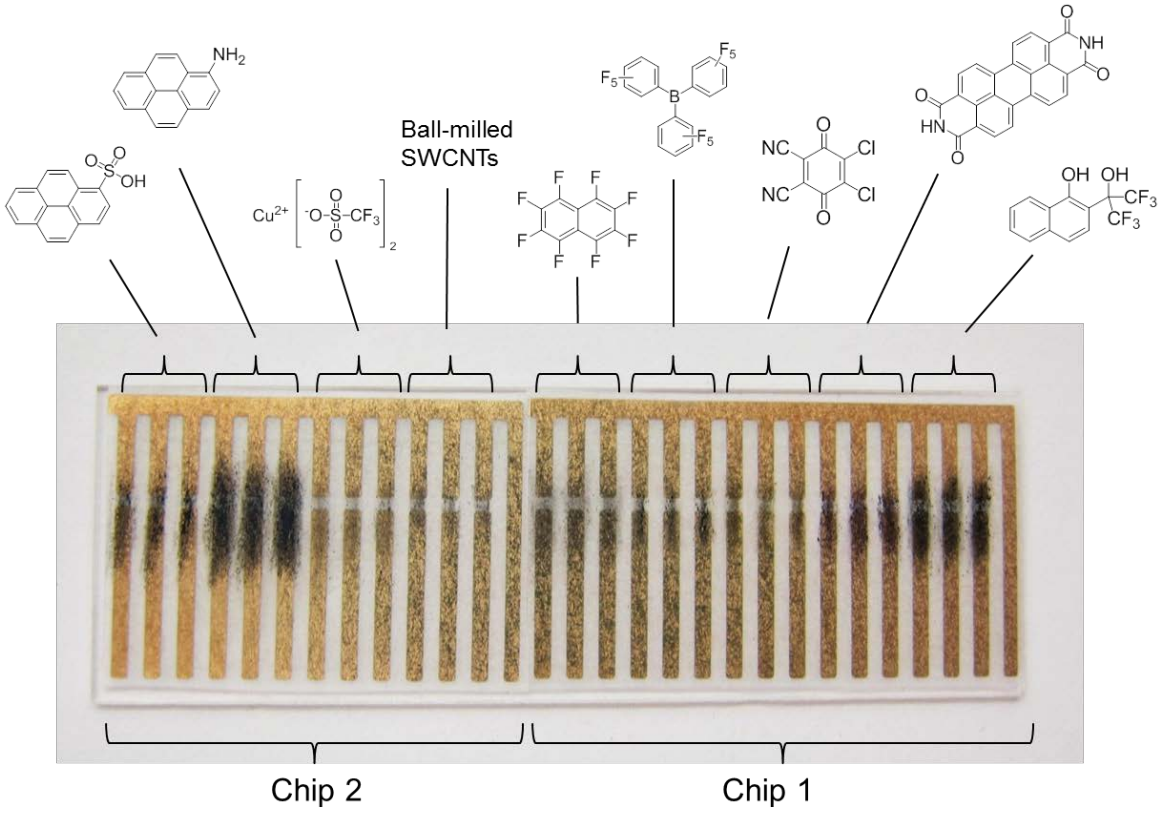

Figure S8. Sensing response ($-\Delta G/G_0$, %) with time of SWCNT-based array towards various analytes. No baseline correction. Each type of sensor was examined in triplicate. Multiple sensing responses for each type of sensor are overlayed to show reproducibility.

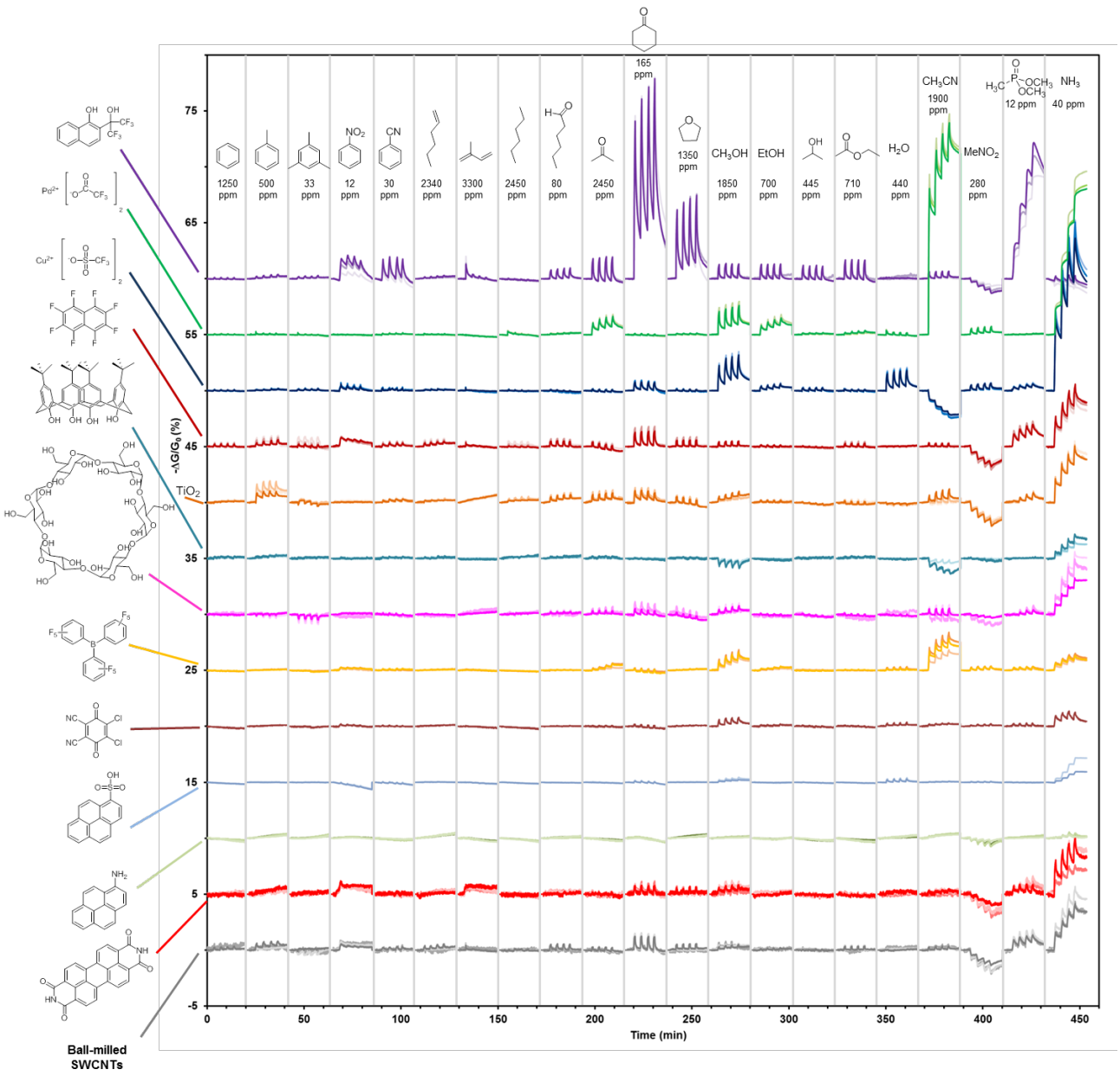

Figure S9. Sensing response ($-\Delta G/G_0$, %) with time of SWCNT-based array towards various analytes. Linear baseline correction was applied to all sensing responses. Each type of sensor was examined in triplicate. Multiple sensing responses for each type of sensor are overlayed to show reproducibility.

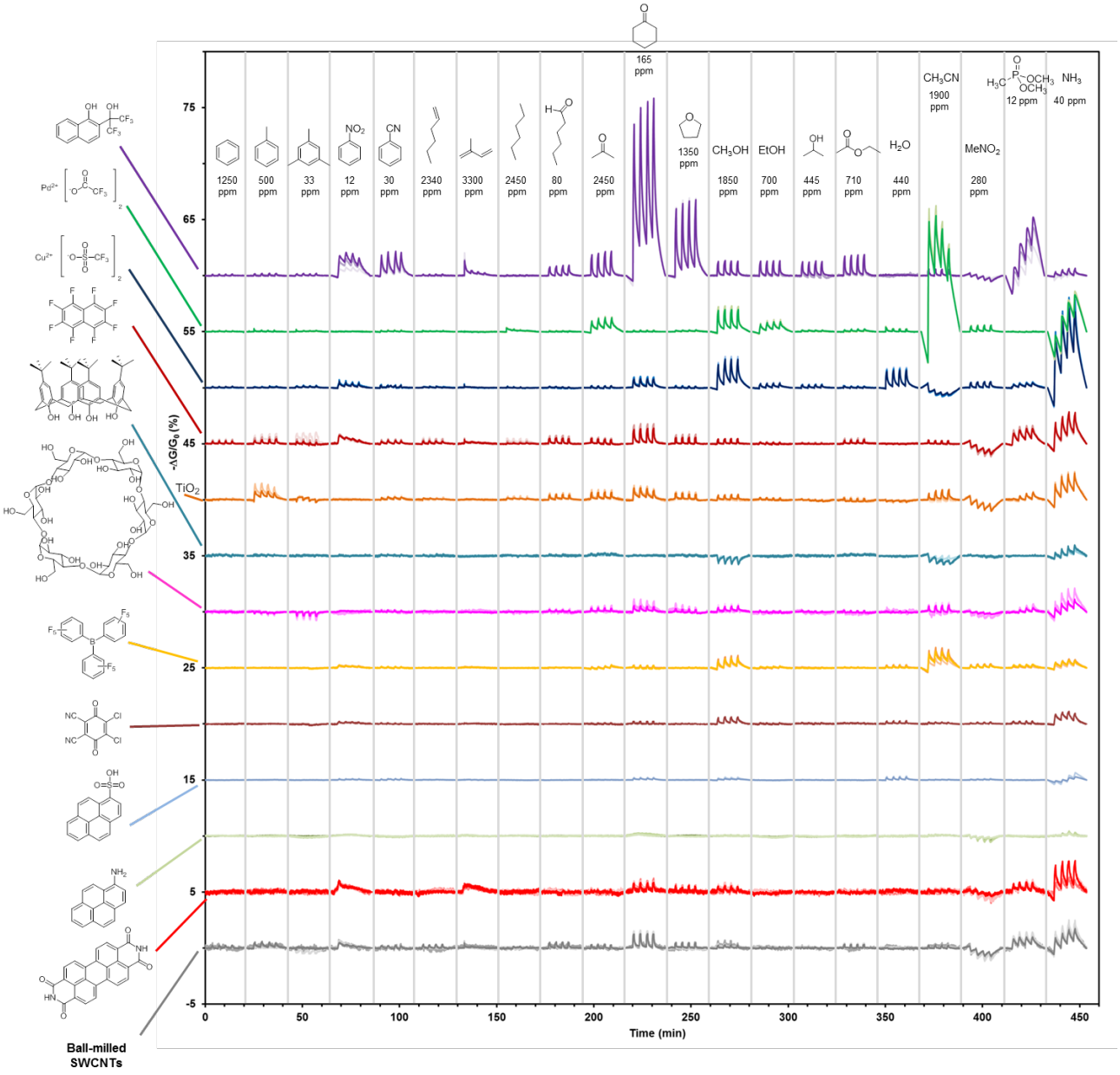

Figure S10. Sensing response ($-\Delta G/G_0$, %) with time of graphite-based array towards various analytes. No baseline correction was applied to the sensing responses. Each type of sensor was examined in triplicate. Multiple sensing responses for each type of sensor are overlayed to show reproducibility.

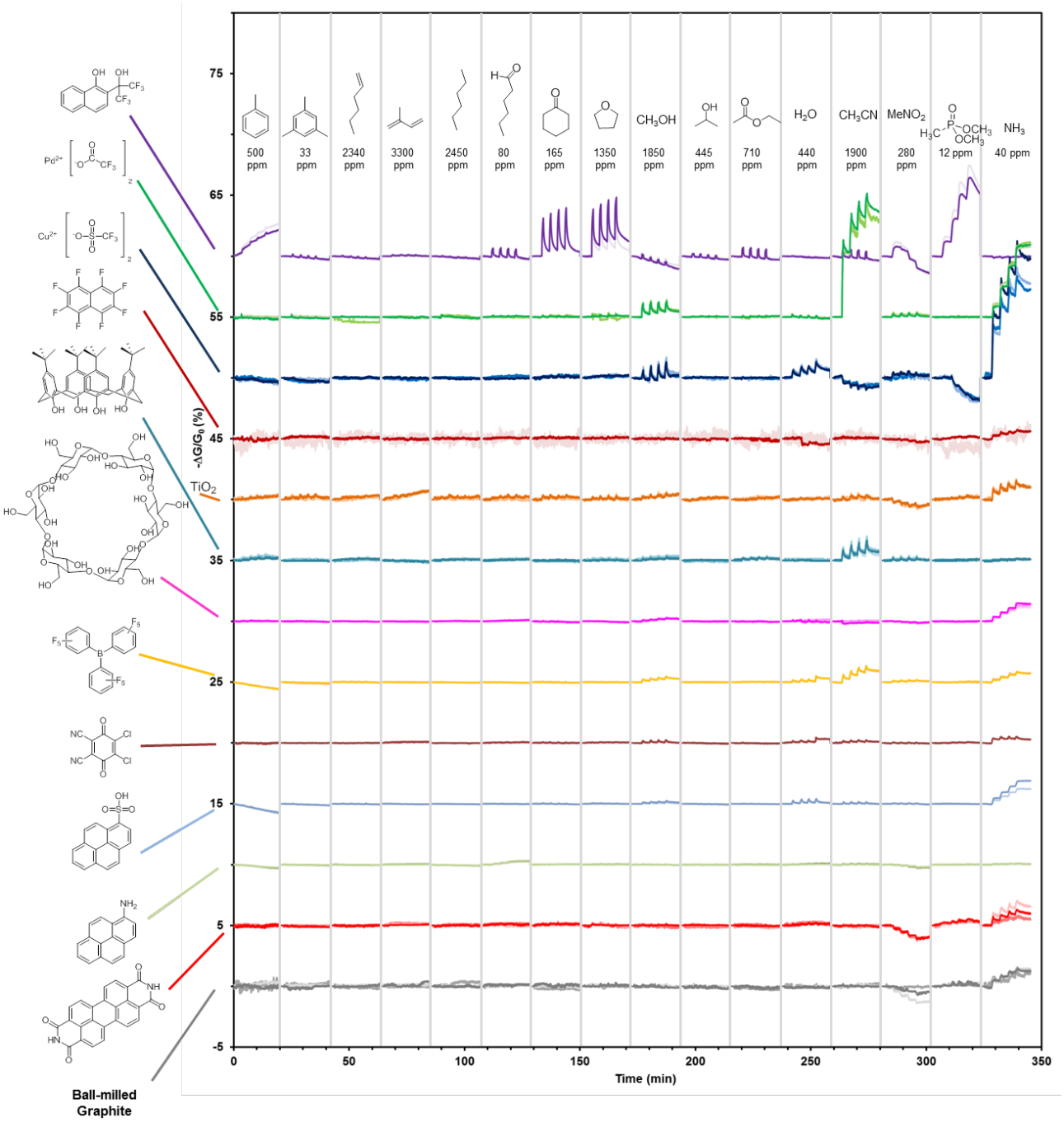

Figure S11. Sensing response ($-\Delta G/G_0$, %) with time of graphite-based array towards various analytes. Linear baseline correction was applied to all sensing responses. Each type of sensor was examined in triplicate. Multiple sensing responses for each type of sensor are overlayed to show reproducibility.

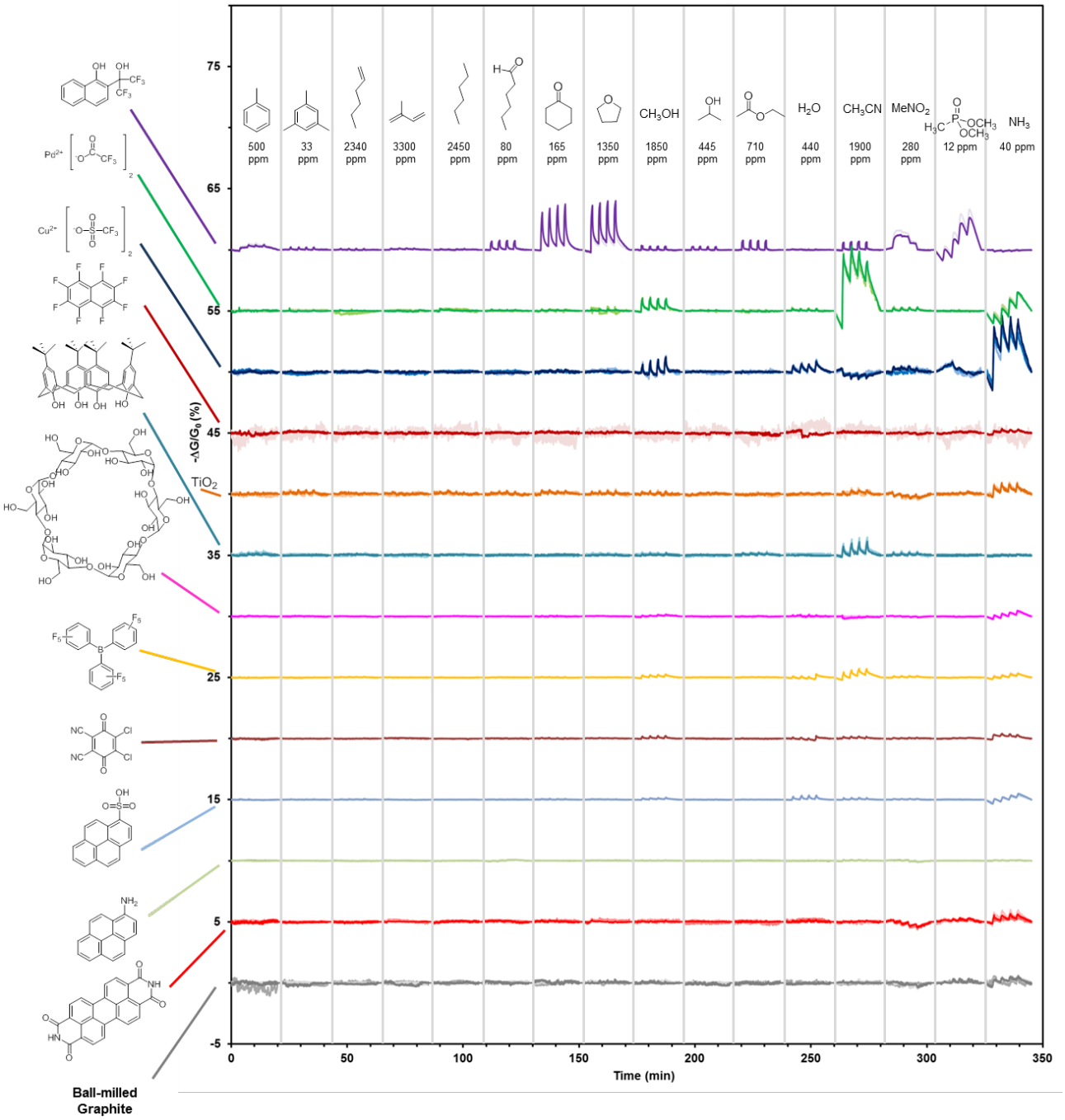

Figure S12. Sensing response of a cross-reactive array fabricated by mechanical abrasion of ball milled and compressed graphite and composites of graphite with selectors S^1–S^4 with (1:4 nC/S by mass) on the surface of weighing paper. Change in conductance (represented as $-\Delta G/G_0$, %) resulting from exposure of the array to eight vapors (at ~ 1 % equilibrium vapor pressure, specific concentrations as shown) and NH_3 gas (40 ppm). Each bar represents the average response of three sensors exposed to each analyte in triplicate. Vertical error bars represent the standard deviation from the average.

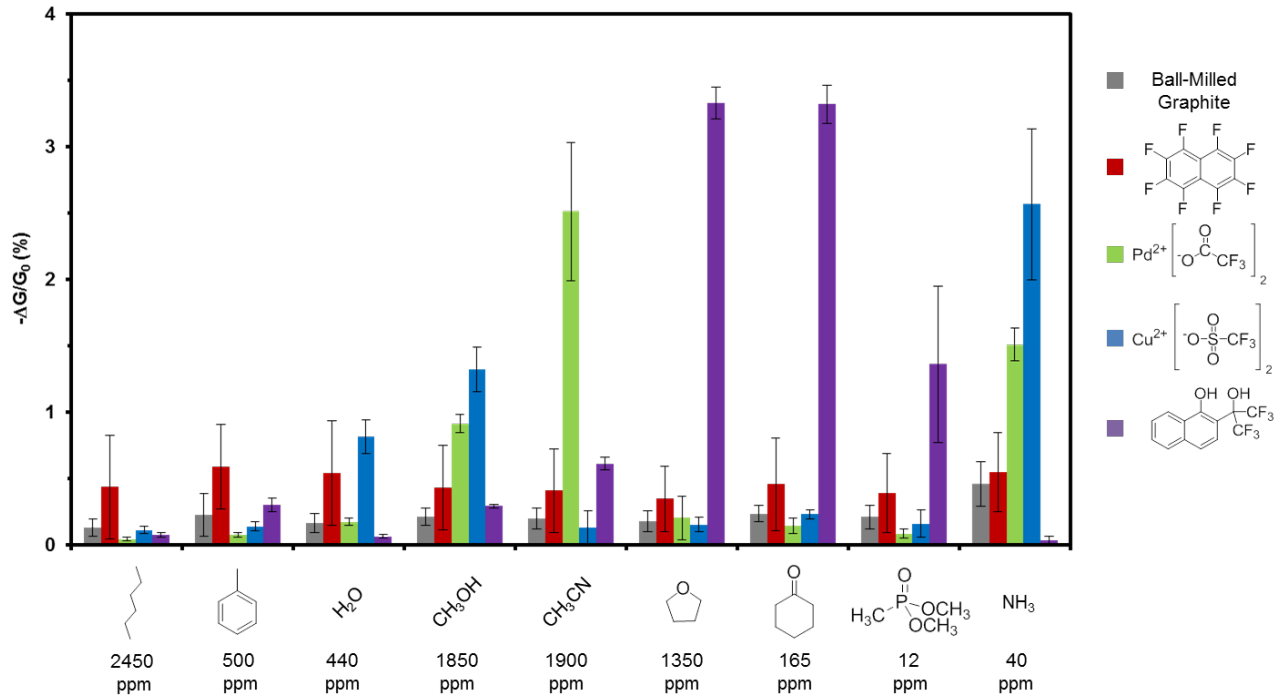

Figure S13. Quantitative comparison of sensing response ($-\Delta G/G_0$, %) toward water (a), ammonia (b), acetonitrile (c), and cyclohexanone (d) of sensors fabricated on the surface of weighing paper by mechanical abrasion of PENCILs comprising compressed blends of graphite and SWCNTs with S^1- S^4 (1:4) by mass. Vertical error bars represent standard deviation from the mean based on three exposures of three sensors to each of the analytes.

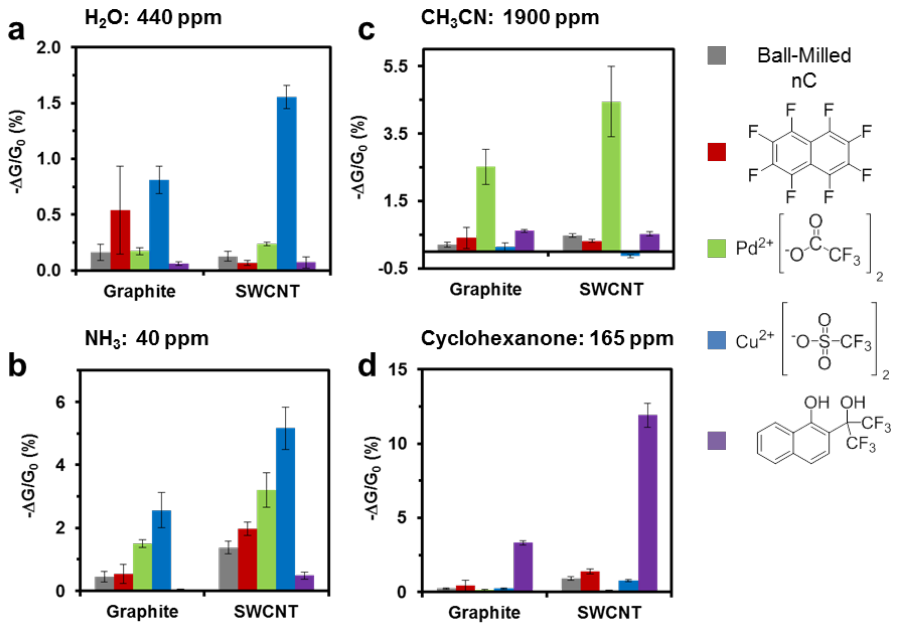

Figure S14. Principal component analysis (PCA) of SWCNT-based array toward ten selected analytes with 3D and 2D projections of principal components.

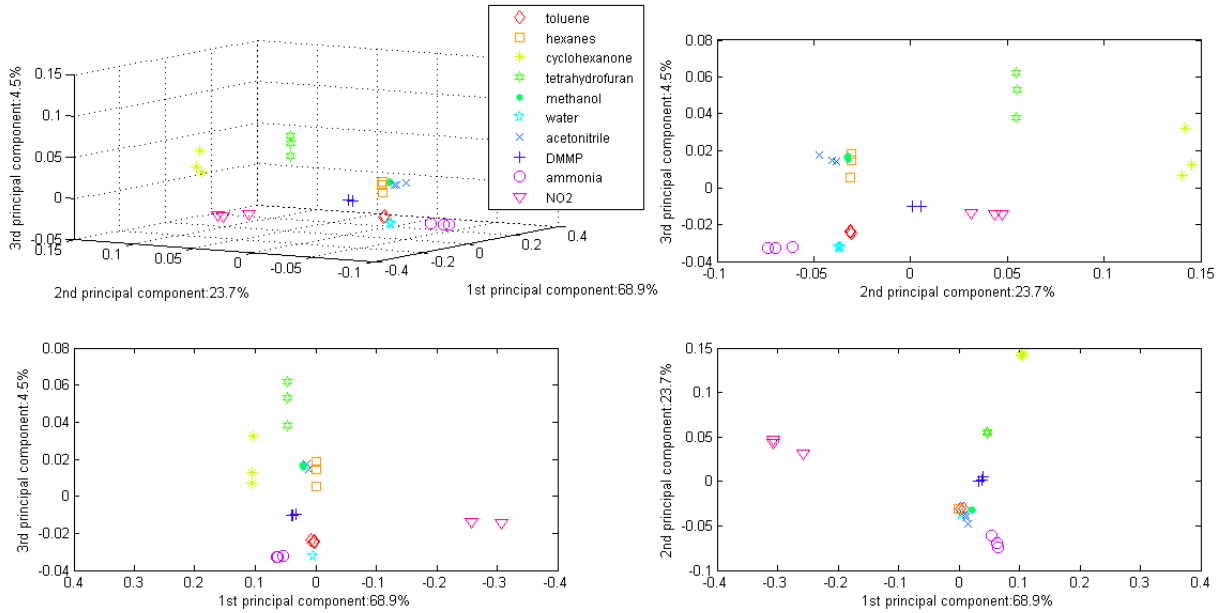

Figure S15A. Principal component analysis (PCA) of the sensing response of the graphite-based array toward nine selected analytes with 3D and 2D projections of principal components.

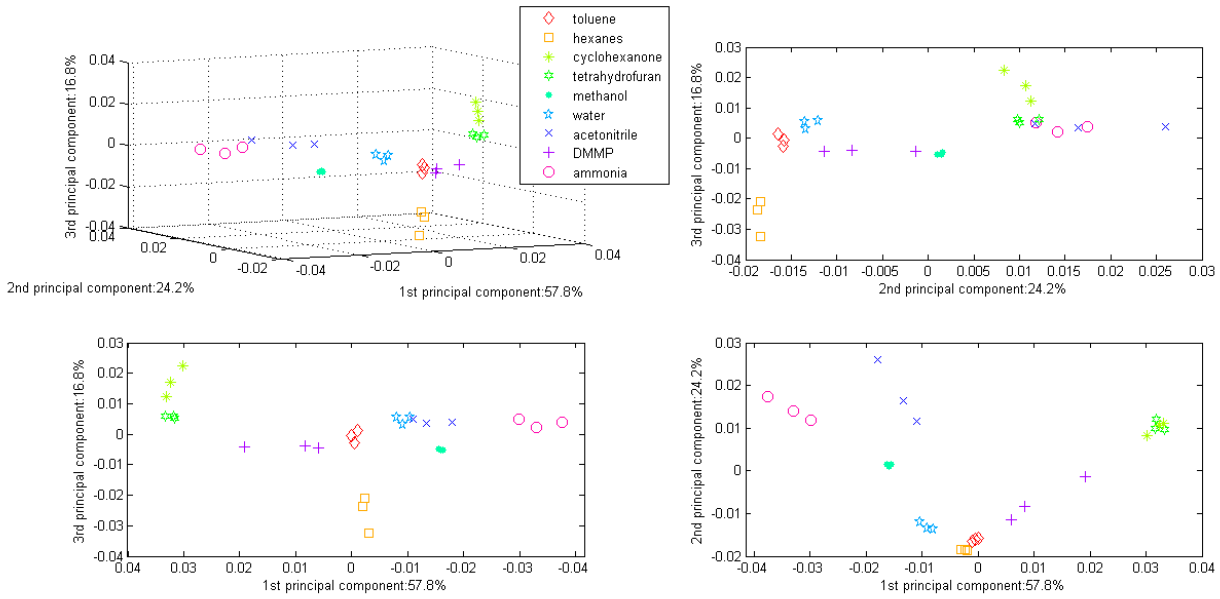

Figure S15B. Principal component analysis (PCA) of the response of SWCNT-based array toward nine selected analytes with 3D and 2D projections of principal components.

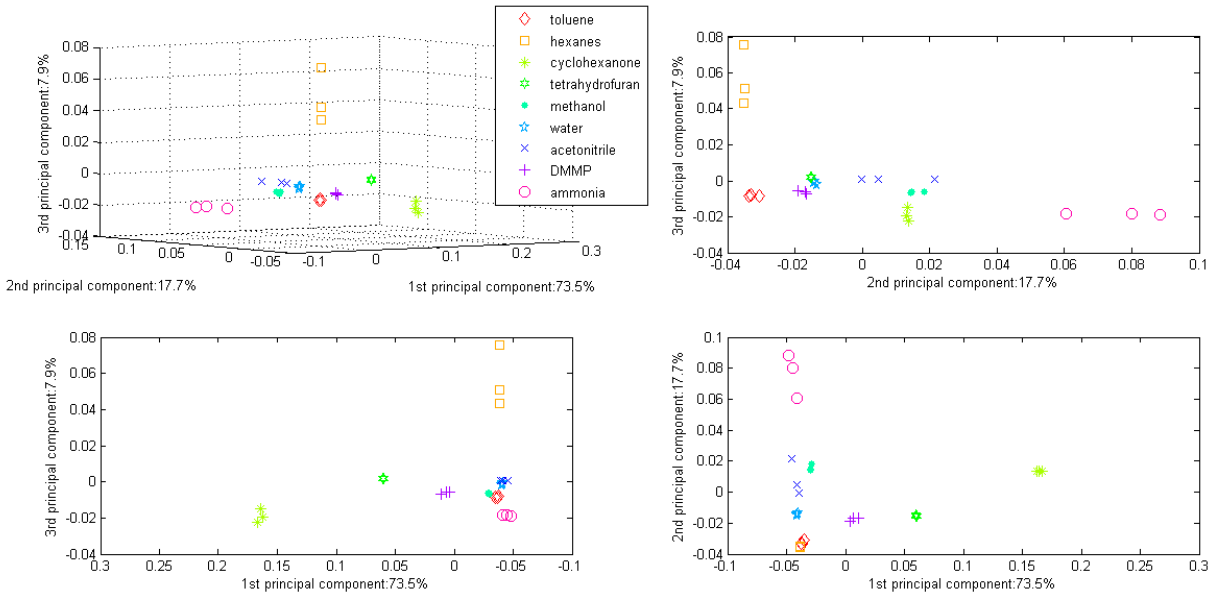

Figure S16. X-Ray survey scans of solid composites of a) SWCNTs/$Cu(OSO_2CF_3)_2$ and b) SWCNTs/$Pd(OCOCF_3)_2$ both 4:1 by mass.

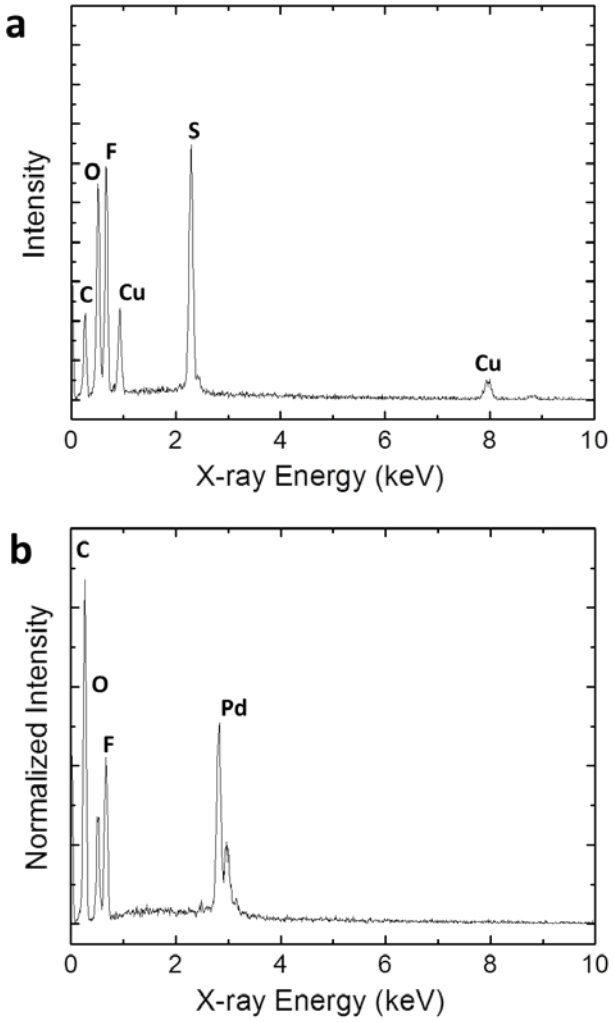

Figure S17. EDX of solid composites of SWCNTs/$Cu(OSO_2CF_3)_2$ and SWCNTs/$Pd(OCOCF_3)_2$ both 4:1 by mass.

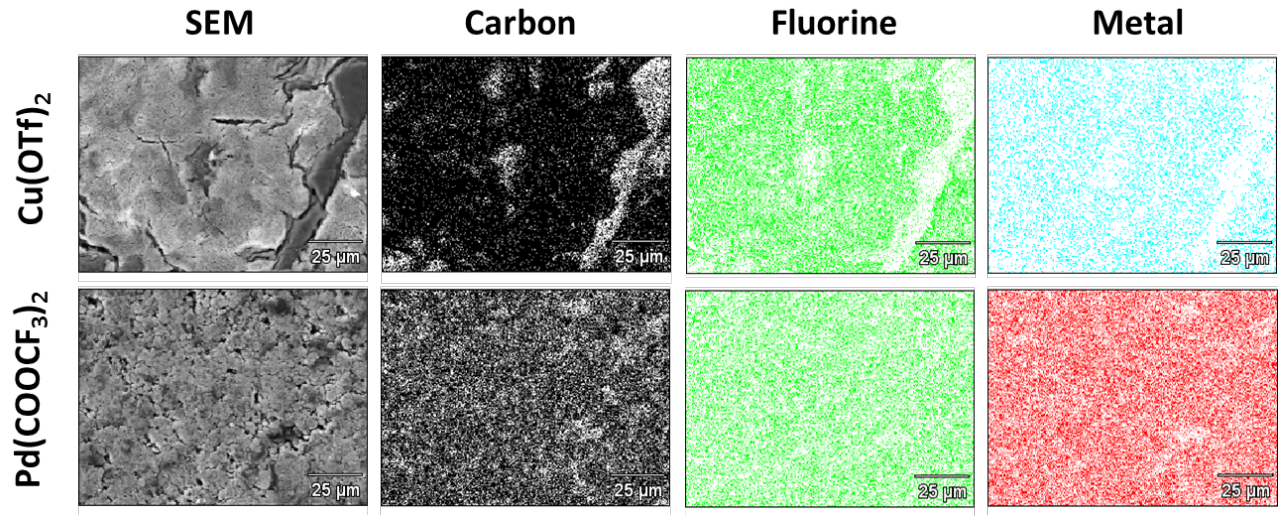

Figure S18. SEM images of solid composites of a) SWCNTs/$Cu(OSO_2CF_3)_2$ and b) SWCNTs/$Pd(OCOCF_3)_2$ both 4:1 by mass.

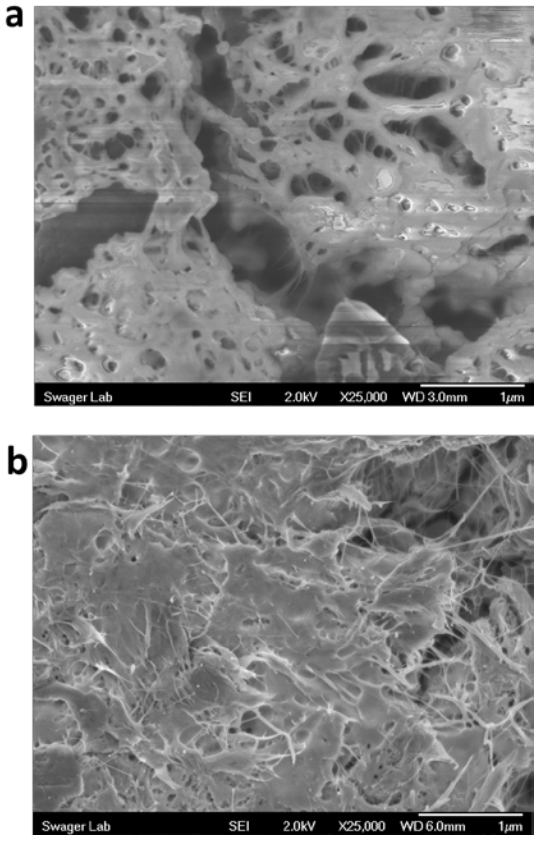

Table S1. Bulk conductivity σ of nC/S[1] composites.

	σ (S/cm)	σ (S/cm)	σ (S/cm)
nC/S[1]	nC = SWCNTs	nC = MWCNTs	nC = Graphite
1 : 0	256 ± 5	14.9 ± 0.2	884 ± 28
1 : 1	56 ± 2	13.1 ± 0.1	82 ± 3
1 : 2	25 ± 1	11.3 ± 0.1	21.9 ± 0.3
1 : 5	2.3 ± 0.1	3.1 ± 0.1	1.4 ± 0.3

Table S2. Hardness (*H*) of nC/S[1] composites.

	H (MPa)	*H* (MPa)
nC/S[1]	nC = SWCNTs	nC = Graphite
1 : 0	118 ± 53	478 ± 262
1 : 1	160 ± 62	21 ± 7
1 : 2	59 ± 34	98 ± 57
1 : 5	7 ± 4	176 ± 72

Table S3. Bulk conductivity σ of 1:4 nC/S composites used for rapid prototyping of sensing arrays.

	σ (S/cm)	σ (S/cm)
S (Scheme 1)	nC = SWCNTs	nC = Graphite
1	2.2 ± 0.2	3.13 ± 0.03
2	17 ± 1	35 ± 2
3	8 ± 7	0.61 ± 0.07
4	48 ± 7	11 ± 2
5	43 ± 8	4.0 ± 0.1
6	0.32 ± 0.02	0.91 ± 0.04
7	12.5 ± 0.2	3.0 ± 0.2
8	8.0 ± 0.3	11.5 ± 0.2
9	19 ± 3	18.8 ± 0.5
10	28 ± 1	3.2 ± 0.1
11	0.20 ± 0.01	40 ± 3
12	30 ± 3	8.4 ± 0.1

References:

1. Collins, WR, Schmois, E and Swager, TM (2011) Graphene oxide as an electrophile for carbon nucleophiles. *Chem Comm* **47:** 8790-8792.

2. Smits, FM (1958) Measurement of sheet resistivities with the four-point probe. *Bell Syst Tech J* **May:** 711-718.